Inorganic Chemistry

Article

pubs.acs.org/IC

Positively Charged Lanthanide Complexes with Cyclen-Based Ligands: Synthesis, Solid-State and Solution Structure, and Fluoride Interaction

Luís M. P. Lima,[†] Alexandre Lecointre,[‡] Jean-François Morfin,[†] Andrés de Blas,[§] Dimitris Visvikis,[†] Loïc J. Charbonnière,*[,‡] Carlos Platas-Iglesias,*[,§] and Raphaël Tripier*[,†]

[†]Université de Bretagne Occidentale, UMR-CNRS 6521/IFR148 ScInBioS, UFR des Sciences et Techniques, 6 avenue Victor le Gorgeu, CS 93837, 29238 Brest Cedex 3, France

[‡]Laboratoire d'Ingénierie Moléculaire Appliquée à l'Analyse, UMR 7178 CNRS/UdS, IPHC, ECPM, 25 rue Becquerel, 67087 Strasbourg Cedex, France

[§]Departamento de Química Fundamental, Universidade da Coruña, Campus da Zapateira, Rúa da Fraga 10, 15008 A Coruña, Spain

Supporting Information

ABSTRACT: The syntheses of a new cyclen-based ligand $\mathbf{L^2}$ containing four *N*-[2-(2-hydroxyethoxy)ethyl]acetamide pendant arms and of its lanthanide(III) complexes $[Ln\mathbf{L^2}(H_2O)]Cl_3$ (Ln = La, Eu, Tb, Yb, or Lu) are reported, together with a comparison with some Ln^{III} complexes of a previously reported analogue $\mathbf{L^1}$ in which two opposite amide arms have been replaced by coordinating pyridyl units. The structure and dynamics of the La^{III}, Lu^{III}, and Yb^{III} complexes in solution were studied by using multinuclear NMR investigations and density functional theory calculations. Luminescence lifetime measurements in H_2O and D_2O solutions of the $[Ln(\mathbf{L^2})(H_2O)]^{3+}$ complexes (Ln = Eu or Tb) were used to investigate the number of H_2O molecules coordinated to the metal ion, pointing to the presence of an inner-sphere H_2O molecule in a buffered aqueous solution. Fluoride binding to the latter complexes was investigated using a combination of absorption spectroscopy and steady-state and time-resolved luminescence spectroscopy, pointing to a surprisingly weak interaction in the case of $\mathbf{L^2}$ ($\log K = 1.4 \pm 0.1$). In contrast to the results in solution, the X-ray crystal structure of the lanthanide complex showed the ninth coordination position occupied by a chloride anion. In the case of $\mathbf{L^1}$, the X-ray structure of the $[(Eu\mathbf{L^1})_2F]$ complex features a bridging fluoride donor with an uncommon linear Eu−F−Eu entity connecting two almost identical $[Eu(\mathbf{L^1})]^{3+}$ units. Encapsulation of the F^- anion within the two complexes is assisted by $\pi-\pi$ stacking between the pyridyl rings of two complexes and C−H···F hydrogen-bonding interactions involving the anion and the pyridyl units.

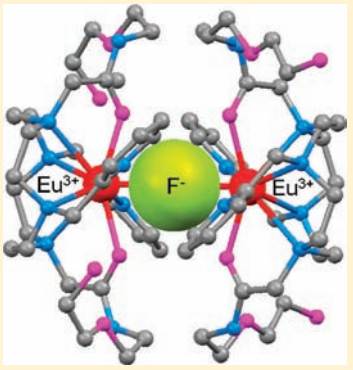

INTRODUCTION

Fluoride sensing is currently attracting particular interest because of the important applications of this anion in dental care by fluoridation of drinking water,[1] in osteoporosis treatment,[2] for ^{18}F-based positron emission tomography,[3] and as a food additive.[4] Furthermore, above certain concentrations, fluoride has been related to health troubles,[5] and its sensing is also of importance for chemical and nuclear warfare agents.[6] Consequently, there is a growing need for the development of selective and sensitive methods for the detection of F^- anions, particularly in aqueous solutions. However, fluoride detection in aqueous solution constitutes a difficult task because the sensor has to compete with the strong hydrogen-bonding network formed with water, and a suitable fluoride sensor should be able to detect fluoride in the presence of other competing anions. Among the different systems reported for fluoride recognition, the vast majority use hydrogen-bonding interactions provided by amide,[7] sulfonamide,[8] indole,[9] catechol,[10] (thio)urea,[11] pyrrole,[12] imidazolium,[13] or positively charged ammonium groups.[14] Recently, fluoride sensing using anion−π interactions has also been reported.[15] Another class of well-documented fluoride sensors is that containing a Lewis acid center such as boron-containing π-electron systems,[16] which can coordinate this anion in aqueous solution below the maximum contaminant level of 4 ppm set by the Environmental Protection Agency.[17] Other receptors are those containing a metal center, such as Li^{I},[18] Cu^{II},[19] Hg^{II},[20] Al^{III},[21] or UO_2^{2+},[22] as the binding site for fluoride.

Lanthanide cations (Ln^{III}) are classified as hard Lewis acids in the Pearson HSAB classification,[23] and therefore the design of fluoride sensors containing these ions as the binding site could be envisaged. Among the lanthanides of interest, those enabling a simple and sensitive fluorimetric detection, such as Eu^{III} and Tb^{III}, are particularly relevant. The use of luminescent lanthanide complexes for anion sensing is a well-established field of spectroscopy.[24] In addition to conventional data collected from the intensity variations due to anion binding,[25]

Received: July 8, 2011
Published: November 9, 2011

the changes occurring in the linelike emission spectra of lanthanides can reveal important features on the binding.[26] Spectral properties such as the luminescence lifetime of the species,[27] polarized absorption,[28] or circularly polarized emission[29] can also be used to monitor the anion-binding interactions. The sensing of fluoride anions by luminescent lanthanide complexes has also been well documented in the literature,[29c,30] and the replacement of water molecules by these anions was even used in lanthanide-based fluoroimmunoassays to improve the luminescence properties of some europium labels.[31]

Cyclen-based lanthanide complexes offer an attractive platform for the development of anion receptors. Indeed, cyclen derivatives with coordinating pendant arms such as DOTA, DOTAM, and DTMA (Chart 1) are known to form some of the most

Chart 1. Ligands Discussed in the Present Work

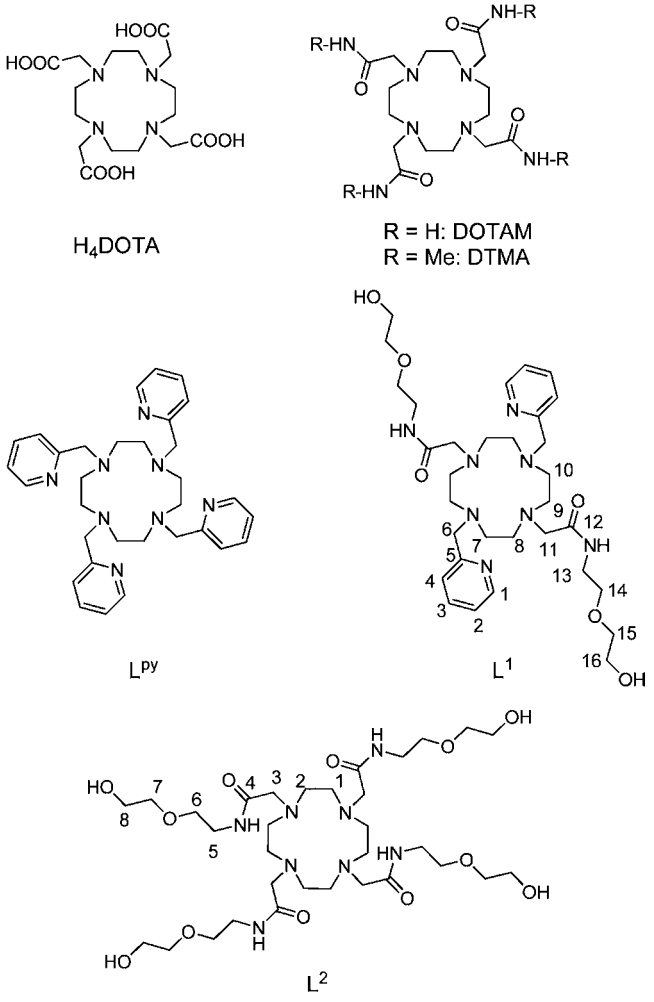

thermodynamically stable and kinetically inert lanthanide complexes.[32] Furthermore, by careful design of the type and number of the coordinating pendants appended on the cyclen backbone, it is possible to obtain coordinatively unsaturated water-soluble lanthanide complexes with one or two coordination positions occupied by water molecules.[32] The reversible displacement of these water molecules from the lanthanide center of the complex has been successfully applied to develop sensors/receptors for a range of meaningful anions.[25a,c,33]

Faulkner et al. have recently reported the synthesis of lanthanide complexes with the ligand 1,4,7,10-tetrakis-(2-pyridylmethyl)-1,4,7,10-tetraazacyclododecane (L^{py}; Chart 1), which contains eight N atoms in its donor set and incorporates four pyridyl chromophores, which can be used to sensitize metal-centered luminescence from a variety of lanthanides.[34] In a recent report, we investigated the complexes of Ln^{III} ions with the macrocyclic receptor $\mathbf{L^1}$ (Chart 1), which is based on a cyclen framework functionalized with 2-methylpyridyl pendants at the 1 and 7 N atoms and with *N*-[2-(2-hydroxyethoxy)-ethyl]acetamide groups at the 4 and 10 N atoms.[35] The triply charged $[Ln(\mathbf{L^1})(H_2O)]^{3+}$ complexes were shown to interact with fluoride anions with very good selectivity over chloride or bromide. Fluoride coordination displaces the apical water molecule in the complex without major perturbation of the coordination sphere, which results in an enhanced Eu^{III}-centered emission upon formation of the ternary complex. In an effort to further understand the parameters governing the interactions with fluoride anions, we now report a detailed investigation of the Ln^{III} complexes of the ligand containing four *N*-[2-(2-hydroxyethoxy)ethyl]acetamide pendants $\mathbf{L^2}$ (Chart 1). The structure and dynamics of the complexes in solution were studied by using a combination of NMR investigations, density functional theory (DFT) calculations, and spectroscopic means. For comparative purposes, these investigations were extended to the $[Ln(\mathbf{L^1})(H_2O)]^{3+}$ complexes. The solid-state structures of the La^{III} complex of $\mathbf{L^2}$ and a fluoride adduct of the Eu^{III} complex of $\mathbf{L^1}$ are also reported.

RESULTS AND DISCUSSION

Synthesis of $\mathbf{L^2}$ and Its Lanthanide Complexes. The synthetic procedure used for the preparation of $\mathbf{L^2}$ is outlined in Scheme 1. Compound **1**[36] was reacted with propionyl chloride using pyridine as a base to give compound **2** after purification by chromatography, as confirmed by analysis of the chemical shifts observed in the NMR spectra, microanalysis, and mass spectrometry (Figures S1−S4, Supporting Information). N-Alkylation of cyclen with **2** at room temperature in acetonitrile in the presence of K_2CO_3 gave compound **3** in good yield (67%), and the subsequent hydrolysis of the propionic ester groups afforded $\mathbf{L^2}$ (Figures S5−S8, Supporting Information) with an overall yield of 41% as calculated from compound **1**. The Ln^{III} complexes of $\mathbf{L^1}$ and $\mathbf{L^2}$ were obtained by mixing equimolar amounts of the ligand with hydrated lanthanide chloride salts in methanol under gentle heating. The mass spectra of the isolated complexes confirmed the $[Ln\mathbf{L}^i]^{3+}$ (i = 1, 2) composition with peaks corresponding to the molecular cation and cations arising from complex fragmentation (Figures S9 and S10, Supporting Information).

Photophysical Properties. In ultrapure water, the UV−vis absorption spectra of the Eu^{III} and Tb^{III} complexes of $\mathbf{L^2}$ displayed a weak and broad absorption band between 260 and 300 nm, which, according to the values of the corresponding molar absorption coefficient, may be attributed to n → π^* transitions centered on the carboamide functions (Figures 1 and 2). At higher energy, an intense absorption band is observed with maxima at 227 (ε = 15 800 M^{-1} cm^{-1}) and 228 nm (ε = 15 000 M^{-1} cm^{-1}), respectively, for Eu^{III} and Tb^{III}, probably arising from π → π^* transitions on the carbonyl functions. Upon excitation into the UV domain, both complexes display the typical emission spectra associated with Ln^{III}-centered emission.

In the case of Eu^{III} (Figure 1), the metal-based emission is composed of the characteristic $^5D_0$ → ^7F_J transitions, with J = 0 (580 nm), 1 (585−601 nm), 2 (607−632 nm), 3 (weak, pointing at 654 nm), and 4 (679−709 nm).[37] Two important

dx.doi.org/10.1021/ic201447c | Inorg. Chem. 2011, 50, 12508−12521

Scheme 1. Synthesis of L^{2a}

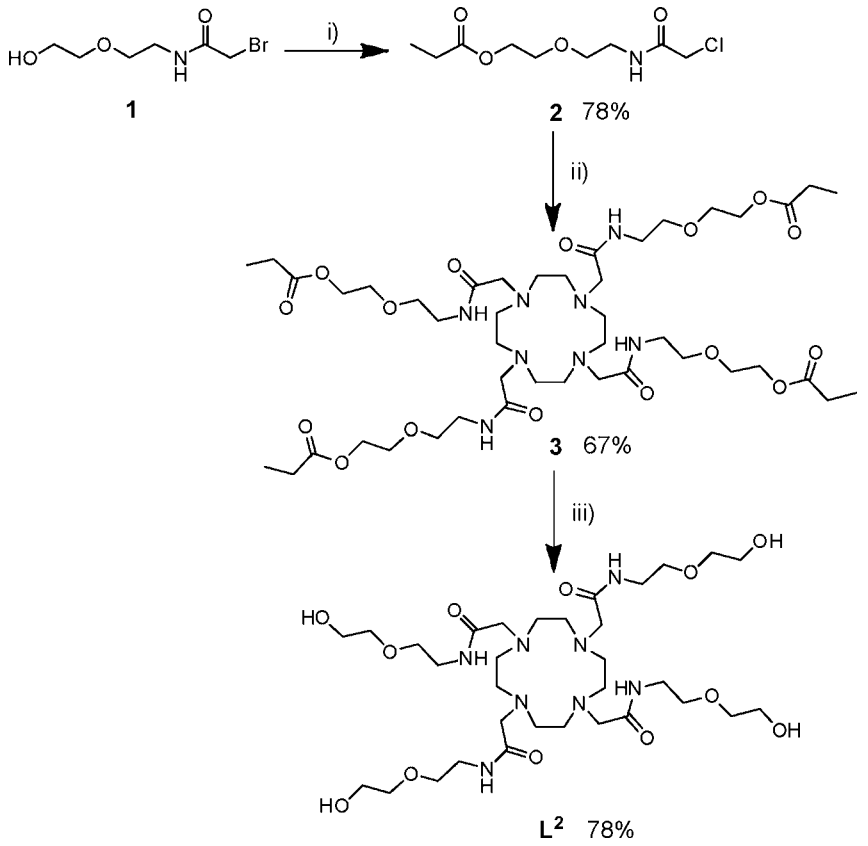

[a]Reaction conditions: (i) propionyl chloride, pyridine; (ii) 1,4,7,10-tetraazacyclododecane, NaI, K_2CO_3/CH_3CN; (iii) 2 M HCl.

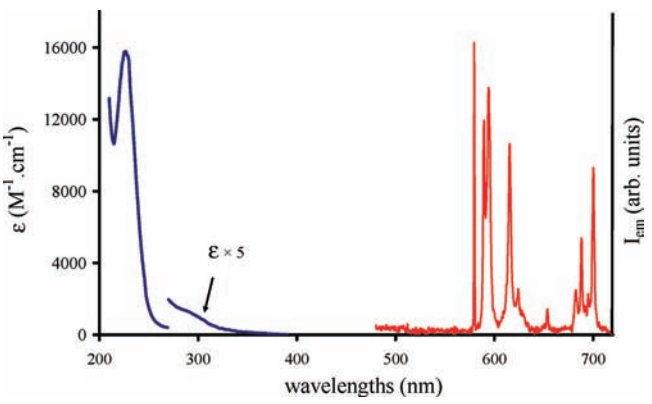

Figure 1. UV−vis absorption (blue) and fluorescence (red, λ_{exc} = 260 nm, cutoff filter at 370 nm) spectra of $[Eu(\mathbf{L}^2)(H_2O)]Cl_3$ in ultrapure water.

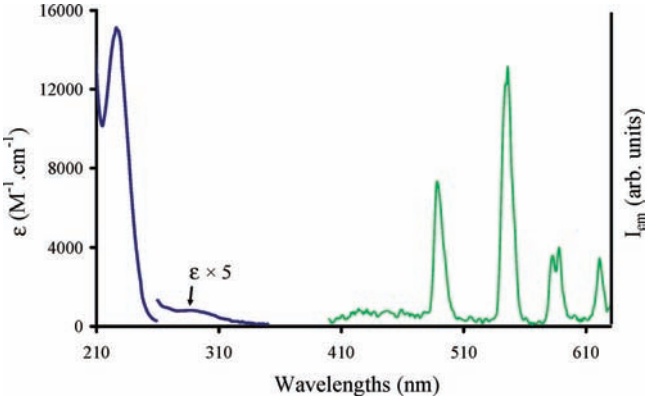

Figure 2. UV−vis absorption (blue) and fluorescence (green, λ_{exc} = 260 nm, cutoff filter at 370 nm) spectra of $[Tb(\mathbf{L}^2)(H_2O)]Cl_3$ in ultrapure water.

features can be noticed from the spectrum. First, the $^5D_0 \rightarrow {}^7F_1$ transition is composed of only two sublevels, in perfect agreement with a C_4 symmetry of the complex in solution. Regarding the weak splitting between the A and E components of this transition ($\Delta E = 128 \pm 15$ cm^{-1}), analysis of structurally relevant DOTA-type complexes of Eu^{III} suggests a twisted square-antiprismatic (TSAP) conformation as the major isomer.[38] Then, in accordance with this symmetrical environment, the $^5D_0 \rightarrow {}^7F_2$ transition is very weak relative to the magnetic dipole-allowed $^5D_0 \rightarrow {}^7F_1$ transition ($I_{0\rightarrow2}/I_{0\rightarrow1} = 1.13$). When the methodology developed by Werts et al. was applied,[39] the radiative lifetime of the Eu^{III} complex was determined to be 9.6 ms. The luminescence lifetimes of the Eu^{III} complex were also determined in ultrapure water, Tris/HCl buffer (pH = 7.0, 0.01 M), and D_2O and amount respectively to 0.56, 0.52, and 2.05 ms. The overall luminescence quantum yield (upon excitation into the ligand absorption bands) was determined relative to $[Ru(bipy)_3]Cl_2$ in nondeoxygenated water (ϕ = 2.8%)[40] and amounts to 2.0(3) × 10^{-3}. The metal-centered luminescence quantum yield can then be calculated using

$$\varphi_{Eu} = \tau_{obs}/\tau_{rad} = 0.058$$

dx.doi.org/10.1021/ic201447c | Inorg. Chem. 2011, 50, 12508–12521

This reveals that the overall very weak luminescence of the complex is due not only to a bad energy transfer from the ligand to the Eu^{III} cation (η_{sens} = 3.5%) but also to a very poor Eu^{III}-centered luminescence, probably resulting from the conjugated quenching effect of OH oscillators from water molecules and CH and CONH ones from the ligand itself.[41]

From the luminescence lifetime in water and heavy water, it was possible to calculate the hydration number of the complex. Taking into account the contributions of OH and CONH oscillators and outer-sphere water molecules, a value of 1.2 ± 0.1 water molecules was obtained using the equation derived by Horrocks for a set of different ligands,[42] while the use of Parker's equation for the same contributions, but obtained from DOTA-like complexes,[41] led to a value of 1.1 inner-sphere water molecules, closer to the expected q = 1 value for an overall coordination number of 9 provided by the octadentate ligand and an inner-sphere water molecule.

The fluorescence spectrum of the Tb^{III} complex also displays the typical emission bands arising from the $^5D_4 \rightarrow {}^7F_J$ transitions with maxima at 488 (J = 6), 546 (J = 5), 588 (J = 4), and 621 (J = 3) nm. The overall luminescence quantum yield was determined to be also rather weak for the Tb complex with a value of $1.5(3) \times 10^{-2}$ (relative to the $[TbL(H_2O)]$ complex in nondeoxygenated water).[43] The luminescence lifetime of Tb^{III} in water amounts to 1.71 ms, and thanks to the lifetime in heavy water (τ_{D_2O} = 2.78 ms), it was possible to calculate the hydration number by taking into account the contribution of outer-sphere water molecules,[41] q = 0.8 ± 0.2. This reveals the presence of a single water molecule in the first coordination sphere of Tb^{III}, in agreement with the results obtained for the Eu^{III} analogue.

Structure and Dynamics of the Complexes in Solution. The ^1H and ^{13}C NMR spectra of the $[Lu(\mathbf{L^1})(H_2O)]^{3+}$ and $[Ln(\mathbf{L^2})(H_2O)]^{3+}$ (Ln = La or Lu) diamagnetic complexes were recorded in a D_2O solution (pD = 6.4 for Lu$\mathbf{L^1}$ and Lu$\mathbf{L^2}$ and 6.6 for La$\mathbf{L^2}$). In the case of the La^{III} complex of $\mathbf{L^2}$, the ^1H NMR spectrum recorded at room temperature shows relatively broad signals due to exchange phenomena, as was previously observed for the complex of $\mathbf{L^1}$.[35] By contrast, the ^1H NMR spectra of the Lu^{III} analogues are well-resolved at 298 K (Figure S11, Supporting Information) and show signals corresponding to one major stereoisomeric form of the complex in solution. The proton signals could be assigned on the basis of 2D heteronuclear HMQC and HMBC experiments as well as standard 2D homonuclear COSY experiments (Table S1, Supporting Information). The ^1H NMR spectrum of $[Lu(\mathbf{L^2})(H_2O)]^{3+}$ consists of 10 signals, which points to an effective C_4 symmetry of the complex in solution. This is confirmed by the ^{13}C NMR spectrum, which shows 8 signals for the 32 carbon nuclei of the ligand backbone. The ^1H and ^{13}C NMR spectra of the $\mathbf{L^1}$ analogue show 20 and 16 signals, respectively, in agreement with an effective C_2 symmetry of the complex in solution.

The binding of a ligand to a paramagnetic Ln^{III} ion provokes relatively large NMR frequency shifts at the ligand nuclei, with magnitudes and signs depending on both the nature of the lanthanide ion and the location of the nucleus relative to the metal center.[44] The hyperfine ^1H NMR shifts in Yb^{III} complexes are considered to be largely pseudocontact in origin, and they can provide useful structural information in solution. For a given nucleus i, the isotropic paramagnetic shift induced by Yb^{III} (δ_i^{para}) can be approximated by the following equation:

$$\delta_i^{dip} = D_1 \frac{3\cos^2\theta - 1}{r^3} + D_2 \frac{\sin^2\theta \cos 2\phi}{r^3} \quad (1)$$

where r, θ, and φ are the spherical coordinates of the observed nucleus with respect to Yb^{III} at the origin and D_1 and D_2 are proportional, respectively, to the axial $[\chi_{zz} - {}^1/_3(\chi_{xx} + \chi_{yy} + \chi_{zz})]$ and rhombic $(\chi_{xx} - \chi_{yy})$ anisotropies of the magnetic susceptibility tensor χ. In the special case of axial symmetry, that is, if the molecule presents a symmetry axis C_n with $n \geq 3$, the second term of eq 1 vanishes because D_2 = 0. The diamagnetic contribution to the observed chemical shifts can be accounted for by measuring the ^1H NMR shifts for the corresponding diamagnetic Lu^{III} complex.

The ^1H NMR spectra of the $[Yb(\mathbf{L^1})(H_2O)]^{3+}$ (Figure 3) and $[Yb(\mathbf{L^2})(H_2O)]^{3+}$ complexes recorded in a D_2O solution

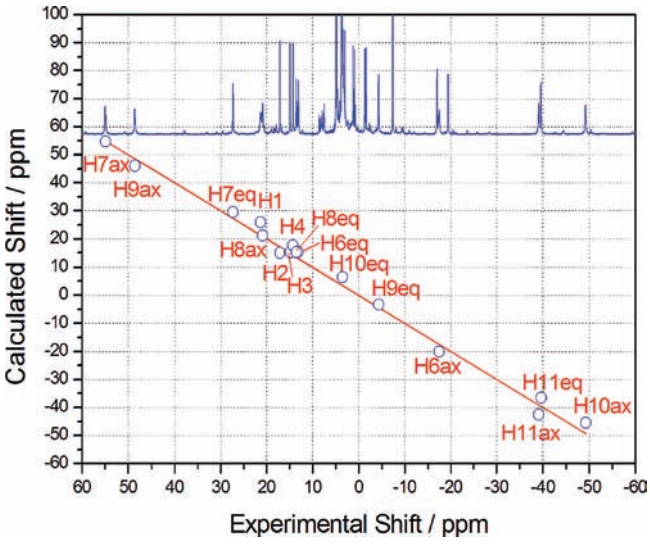

Figure 3. ^1H NMR spectrum of $[Yb(\mathbf{L^1})(H_2O)]^{3+}$ recorded in a D_2O solution (pD = 6.1) at 298 K and plot of experimental versus calculated shifts. The solid line represents a perfect fit between the experimental and calculated values. See Chart 1 for labeling.

(pD = 6.1 and 6.4, respectively) are well resolved. They both show the signals corresponding to a major isomer in solution, together with signals of smaller intensity arising from the presence of a second complex species (<6%). The major species observed in the spectrum of the complex of $\mathbf{L^1}$ shows 21 signals, in agreement with an effective C_2 symmetry of the complex in solution (Table 1). The spectrum of the $\mathbf{L^2}$ analogue is much simpler and presents 11 signals corresponding to the species with the highest abundance, which points to an effective C_4 symmetry of this species in solution. Thus, the magnetic susceptibility tensor of $[Yb(\mathbf{L^1})(H_2O)]^{3+}$ is expected to be rhombic ($D_2 \neq 0$), while that of the $\mathbf{L^2}$ analogue is expected to be axial (D_2 = 0). Analysis of the ^1H NMR shifts in these complexes thereby allows assessment of the effect of the rhombic contribution on the Yb^{III}-induced hyperfine ^1H NMR shifts. The assignments of the proton signals (Table 1) of the major species observed in the spectra of the $[Yb(\mathbf{L^1})(H_2O)]^{3+}$ and $[Yb(\mathbf{L^2})(H_2O)]^{3+}$ complexes were based on standard 2D homonuclear COSY experiments, which gave strong cross-peaks between the geminal CH_2 protons as well as between

dx.doi.org/10.1021/ic201447c | Inorg. Chem. 2011, 50, 12508–12521

Table 1. Comparison of Experimental and Calculated ^{1}H NMR Shifts [ppm with Respect to Tetramethylsilane (TMS)] for the Yb^{III} Complexes of L^1 and L^2 [a]

	L^1			L^2	
	δ_i^{exp}	δ_i^{calc} [b]		δ_i^{exp}	δ_i^{calc} [b]
H1	21.30	25.80	H1ax	96.38	95.29
H2	17.11	14.99	H1eq	17.92	20.70
H3	14.87	15.27	H2ax	−30.85	−27.72
H4	14.24	17.71	H2eq	15.08	18.26
H6ax	−17.50	−20.09	H3ax	−57.63	−60.68
H6eq	13.10	15.35	H3eq	−25.59	−22.36
H7ax	54.94	54.66	H5a	−2.77	e
H7eq	27.26	29.59	H5b	−6.74	e
H8ax	20.87	21.24	H6a	−0.40	e
H8eq	13.54	15.26	H6b	−1.68	e
H9ax	48.54	46.06	H7a	0.95	e
H9eq	−4.34	−3.29	H7b	0.61	e
H10ax	−49.25	−45.47	H8a	1.80	e
H10eq	3.49	6.45	H8b	1.73	e
H11ax	−39.14	−42.53			
H11eq	−39.63	−36.51			
D_1 [c]		−1603			−3291
D_2 [c]		3520			
AF_j [d]		0.088			0.057

[a]The diamagnetic contribution was estimated from the shifts observed for the Lu^{III} analogue. [b]Values calculated by using eq 1 and the SAP conformations of the complexes optimized at the B3LYP/6-31G(d) level. [c]In ppm Å^3. [d]$AF_j = [\sum_i(\delta_i^{exp} - \delta_i^{calc})^2/\sum_i(\delta_i^{exp})^2]^{1/2}$, where δ_i^{exp} and δ_i^{calc} represent the experimental and calculated values of a nucleus i, respectively. [e]Not included in the analysis of the paramagnetic shifts.

vicinal axial−axial protons of the cyclen unit. The ^{1}H NMR peaks due to CH_2 protons of the cyclen moiety and H3 protons in $[Yb(\mathbf{L^2})(H_2O)]^{3+}$, as well as H6 and H11 protons in $[Yb(\mathbf{L^1})(H_2O)]^{3+}$, can be grouped into two different sets according to their relative line broadening: a group of resonances with line widths at half-height of 54−76 Hz (at 300 MHz and 298 K) and a second set of signals with line widths in the range 26−35 Hz (Figure 3). These two sets of signals correspond to two sets of Yb^{III}−H distances, with the broader resonances being associated with the protons closer to the metal ion.[45] Thus, the broader resonances were assigned to axial protons, while the second set of signals was assigned to equatorial ones. A full assignment of the ^{1}H NMR spectra was achieved with the *SHIFT ANALYSIS* program developed by Forsberg et al.,[46] which allows one to perform random permutations of the dipolar shifts.

Aiming to obtain information about the structure in solution of the $[Ln(\mathbf{L^1})(H_2O)]^{3+}$ and $[Ln(\mathbf{L^2})(H_2O)]^{3+}$ complexes, we have performed DFT calculations based on the B3LYP model. On the grounds of our previous experience,[47] in these calculations we have used the effective core potential (ECP) of Dolg et al.[48] and the related [5s4p3d] Gaussian-type orbital (GTO) valence basis set for the lanthanides, while the remaining atoms were described by using the 6-31G(d) basis set. For computational simplicity in these calculations, the 2-(2-hydroxyethoxy)ethyl chains of the ligands were substituted by methyl groups, with the methyl-substituted ligands being denoted as $\mathbf{L^{1\prime}}$ and $\mathbf{L^{2\prime}}$ ($\mathbf{L^{2\prime}}$ actually corresponds to DTMA; see Chart 1). In our previous paper, we reported DFT calculations on the $[Ln(\mathbf{L^1})(H_2O)]^{3+}$ systems (Ln = La or Eu) performed in the gas phase.[35] Herein, we extend these studies to the Yb^{III} complex to obtain structural models for analysis of the paramagnetic Yb^{III}-induced shifts.

It is well-known that in nine-coordinate Ln^{III}DOTA-like complexes the four ethylenediamine groups adopt gauche conformations, giving rise to two macrocyclic ring conformations: ($\delta\delta\delta\delta$) and ($\lambda\lambda\lambda\lambda$). Furthermore, there are two possible orientations of the four pendant arms (absolute configuration Δ or Λ) resulting in four possible stereoisomers, existing as two enantiomeric pairs.[49] These stereoisomers differ by the layout of the four carboxylic arms, adopting either a monocapped square-antiprismatic (SAP) or a monocapped twisted square-antiprismatic (TSAP) geometry.[50] As expected, our calculations provide the SAP and TSAP isomers as minimum-energy conformations for the $[Ln(\mathbf{L^{1\prime}})(H_2O)]^{3+}$ and $[Ln(\mathbf{L^{2\prime}})(H_2O)]^{3+}$ systems. The main calculated geometrical parameters for both isomers are shown in Tables S2 and S3 (Supporting Information). Our calculations reproduce reasonably well the bond distances and angles observed in the solid state for $[Eu_2(\mathbf{L^1})_2F]^{5+}$ and $[La(\mathbf{L^2})Cl]^{2+}$ complexes (see below). The main discrepancy observed between the experimental and calculated structures is the overestimation in the latter of the Ln−N distances by 0.01−0.10 Å and the Ln−O bond lengths by 0.01−0.04 Å. The optimized structures show nearly undistorted C_2 and C_4 symmetries for the complexes of $\mathbf{L^{1\prime}}$ and $\mathbf{L^{2\prime}}$, respectively, with the symmetry axis being perpendicular to the mean plane defined by the N atoms of the cyclen fragment and containing the Ln ion and the O atom of the inner-sphere water molecules. The mean twist angles (Φ) between the two parallel squares range ca. between 34 and 38° and between −19 and −24° in the SAP and TSAP isomers, respectively. These values are very similar to those observed in the solid state for the respective isomers of DOTA complexes.[51] The absolute Φ values increase by ca. 3−5° upon proceeding to the right across the lanthanide series, as the ionic radius of the Ln^{III} ion decreases.

The SAP and TSAP geometries of $[Yb(\mathbf{L^{1\prime}})(H_2O)]^{3+}$ and $[Yb(\mathbf{L^{2\prime}})(H_2O)]^{3+}$ complexes obtained from DFT calculations were used to assess the agreement between the experimental and predicted Yb^{III}-induced paramagnetic shifts with the *SHIFT ANALYSIS* program developed by Forsberg et al.[46] The *SHIFT ANALYSIS* program calculates the dipolar shifts defined by eq 1 in the molecular coordinate system by using a linear least-squares search that minimizes the difference between the experimental and calculated data. The proton signals of the *N*-[2-(2-hydroxyethoxy)ethyl]acetamide groups were excluded from this analysis because their relatively long distance to the paramagnetic center results in small Yb^{III}-induced paramagnetic shifts.

The agreement between the experimental and calculated isotropic shifts obtained by using the SAP isomers was very good (Table 3), while poorer agreement factors were obtained for the TSAP conformations. Table 1 shows the D_1 and D_2 values providing the best fit of the experimental shift values, as well as a comparison of the experimental and calculated paramagnetic shifts according to the dipolar model. The excellent agreement observed between the experimental and calculated Yb^{III}-induced paramagnetic shifts unambiguously proves that these complexes adopt a SAP geometry in aqueous solution. As expected for nonaxial systems, in the case of the $[Yb(\mathbf{L^1})(H_2O)]^{3+}$ complex, the calculated D_1 and D_2 values define a rhombic magnetic susceptibility tensor, while for the $\mathbf{L^2}$ analogue, a good fit of the experimental data was obtained by using an axial model. The D_1 values obtained from the fitting of the paramagnetic shifts observed for the complexes of $\mathbf{L^1}$ and

dx.doi.org/10.1021/ic201447c | Inorg. Chem. 2011, 50, 12508−12521

L^2 are very different, indicating that replacement of the amide groups of the ligand by pyridyl pendant arms has a strong effect on the magnetic susceptibility tensor of this system, which is related to the second-order crystal-field parameters of the complex.

The ^{13}C NMR spectrum of $[Lu(L^1)(H_2O)]^{3+}$ recorded at 278 K shows two signals due to the carbon nuclei of the macrocyclic fragment at 58.0 and 58.7 ppm. These signals gradually broaden above this temperature and finally achieve coalescence at ca. 338 K, reflecting intramolecular dynamic exchange processes (Figure 4). This behavior is consistent with

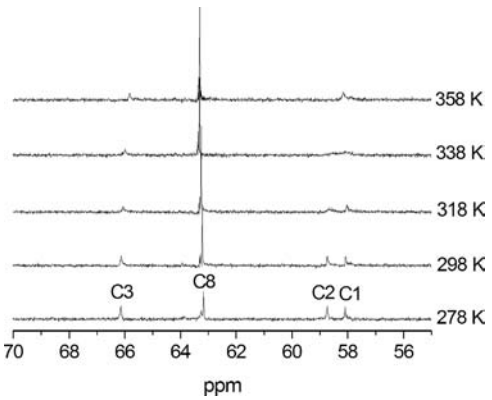

Figure 4. Aliphatic region of the ^{13}C NMR spectra (125.8 MHz) of $[Lu(L^1)(H_2O)]^{3+}$ recorded in a D_2O solution (pD = 6.4) at different temperatures. See Chart 1 for labeling.

an enantiomerization process that interconverts the $\Lambda(\delta\delta\delta\delta)$ and $\Delta(\lambda\lambda\lambda\lambda)$ isomers and represents a simple exchange process between two equally populated sites. This dynamic process involves inversion of the macrocyclic ring, which leads to a $(\delta\delta\delta\delta) \leftrightarrow (\lambda\lambda\lambda\lambda)$ conformational change, and rotation of the four pendant arms of the ligand, resulting in a $\Lambda \leftrightarrow \Delta$ configurational change.[52] If it is assumed that the exchange process associated with the line broadening (before coalescence) is slow on the actual NMR time scale, the exchange rate for this dynamic process (k) can be calculated from $\Delta\nu_{1/2}$, the observed line widths at half-height: $k = \pi[\Delta\nu_{1/2} - \Delta\nu_{1/2}(0)]$, where $\Delta\nu_{1/2}(0)$ is the line width in the absence of exchange. The Eyring plot ($R^2 > 0.994$; Figure S12, Supporting Information) of $\ln(k/T)$ versus $1/T$ in the temperature range 278−333 K, where k is given in eq 2 (χ is the transmission coefficient assumed to be 1, k_B is the Boltzmann constant, T is the absolute temperature, k is the rate constant, and $\Delta G^{\ddagger}$, $\Delta H^{\ddagger}$, and $\Delta S^{\ddagger}$ are the activation free energy, enthalpy, and entropy, respectively) yields the following activation parameters: $\Delta G^{\ddagger} = 66 \pm 8$ kJ mol^{-1}, $\Delta H^{\ddagger} = 33 \pm 3$ kJ mol^{-1}, and $\Delta S^{\ddagger} = -109 \pm 7$ J K^{-1} mol^{-1} at 298 K.

$$k = \chi(k_B T/h)\exp(\Delta S^{\ddagger}/R - \Delta H^{\ddagger}/RT) \quad (2)$$

The free-energy barrier determined from analysis of the NMR spectra is very similar to that determined for the ring-inversion process in different Ln^{III} complexes with cyclen-based ligands. Thus, the rate-determining step for the enantiomerization process in $[Lu(L^1)(H_2O)]^{3+}$ most likely corresponds to the cyclen-inversion pathway. To confirm this, we investigated the ring-inversion and arm-rotation processes in $[Lu(L^{1\prime})(H_2O)]^{3+}$ with the aid of DFT calculations. As previously determined for $[Lu(DOTA)]^-$, our calculations indicate that the arm-rotation process is also a one-step process involving a concerted rotation of the four pendant arms of the ligand (Figure 5). The activation free energy for this process (50.1 kJ mol^{-1}) is lower than that obtained for $[Lu(DOTA)]^-$ using the same computational approach (82 kJ mol^{-1}).[52] These results suggest that replacement of the negatively charged acetate groups of DOTA by neutral acetamide ones results in a substantial lowering of the activation barrier for the arm-rotation process, leading to a $\Lambda \leftrightarrow \Delta$ configurational change. According to our results obtained on B3LYP/6-31G(d)-optimized geometries, the inversion of the cyclen moiety is a four-step process (Figure 5), which is in line with previous computational studies performed on different Ln^{III} complexes with cyclen-based ligands.[52,53] In each of these steps, one five-membered chelate ring changes its configuration from δ to λ, passing through a transition state (TS) in which the chelate ring adopts a nearly planar conformation with the NCCN moiety in eclipsed disposition. Because of the multistage nature of the ring-inversion process, the experimentally measured activation energy would be effective over the four stages shown in Figure 5. The TS endowed with the highest free energy corresponds to TS_3, whose energy (58.6 kJ mol^{-1}) is only slightly lower than that determined experimentally (66 ± 8 kJ mol^{-1}). According to the mechanism proposed in Figure 5, enantiomerization requires interconversion between the SAP and TSAP isomers. Alternatively, the enantiomerization process could follow a pathway involving inversion of two ethylenediamine units to form a $\Lambda(\lambda\delta\lambda\delta)$ intermediate and subsequent rotation of the pendant arms at this point instead of at the end of the ring flip. Once the ring reaches a $(\lambda\delta\lambda\delta)$ conformation, there is no difference in energy between the two possible orientations of the pendant arms. However, the free energy calculated for the TS responsible for the $\Lambda(\lambda\delta\lambda\delta) \leftrightarrows \Delta(\lambda\delta\lambda\delta)$ interconversion, which involves a concerted rotation of the four pendant arms, is considerably high (84.2 kJ mol^{-1}). This supports the fact that the mechanism proposed in Figure 5 on the basis of DFT calculations is basically correct, and the enantiomerization process requires interconversion between the SAP and TSAP isomers. According to our calculations, the rate-determining step for the enantiomerization process corresponds to the ring-inversion pathway. Furthermore, the activation free energies calculated for the arm-rotation and ring-inversion processes are in excellent agreement with those determined experimentally for $[Eu(DTMA)(H_2O)]^{3+}$, which amount to 56.9 kJ mol^{-1} (arm rotation) and 62.2 kJ mol^{-1} (ring inversion).[54]

Fluorescence Titration of $[Eu(L^2)(H_2O)]Cl_3$ by NaF. The interaction of fluoride anions with the Eu^{III} complex was monitored by spectrofluorimetric titration experiments in which the emission spectra of the complex were measured as a function of NaF addition in a buffered water solution (0.01 M Tris/HCl at pH = 7.0). It soon appeared that the interaction was very weak, thereby necessitating large amounts of added fluoride. Figure 6 represents the evolution of the Eu^{III}-based emission spectra as a function of added fluoride. Because of the weakness of the fluorescence signal, it was not possible to obtain a resolution better than 1 nm, but this was sufficient to observe large changes, in particular on the $^5D_0 \rightarrow {}^7F_J$ transitions with $J = 1$ (580−600 nm) and $J = 4$ (680−710 nm). The evolution of the spectra was fitted with the *SPECFIT* software,[55] from which the evolving factor analysis clearly reveals formation of a single new species. The data were then fitted to the following model:

$$[Eu(L^2)(H_2O)]^{3+} + F^- \leftrightarrows [Eu(L^2)F]^{2+} + H_2O$$

dx.doi.org/10.1021/ic201447c | Inorg. Chem. 2011, 50, 12508–12521

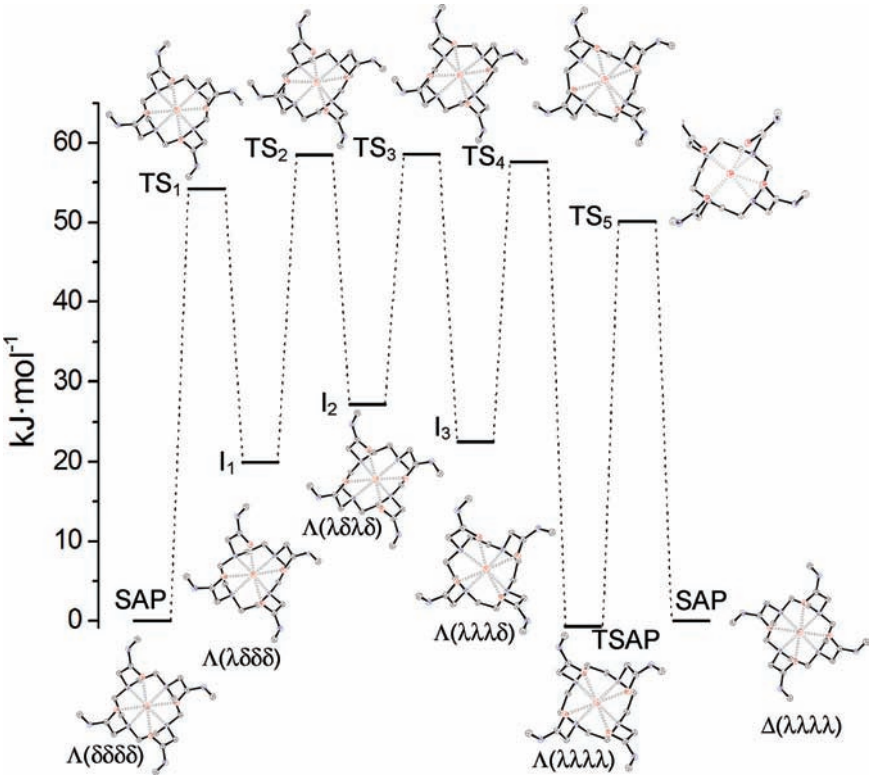

Figure 5. Relative free energies of minima, intermediates (I), and TSs involved in the $\Lambda(\delta\delta\delta\delta) \leftrightarrows \Delta(\lambda\lambda\lambda\lambda)$ enantiomerization process of $[Lu(\mathbf{L}^{1\prime})(H_2O)]^{3+}$.

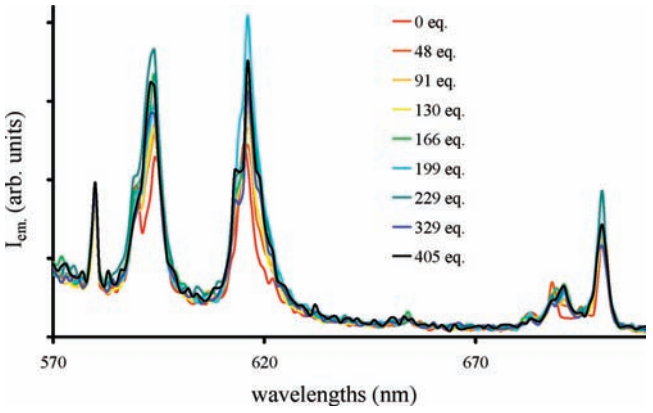

Figure 6. Evolution of the Eu-centered emission spectra of $[Eu(\mathbf{L}^{2})]^{3+}$ as a function of the NaF equivalents added into the solution (λ_{exc} = 280 nm, cutoff filter at 370 nm).

Assuming a constant concentration of water, the apparent stability constant can be written as

$$K = \frac{[(EuLF)^{2+}]}{[(EuL(H_2O))^{3+}][F^-]}$$

The fitting of the data corroborates a very weak association with a log K value of only 1.4 ± 0.1, 2−3 orders of magnitude smaller than those observed for $[Eu(\mathbf{L}^{1})(H_2O)]^{3+}$ [35] or other lanthanide complexes.[56] However, the Mulliken metallic charges obtained from DFT calculations for the $[Eu(\mathbf{L}^{1\prime})(H_2O)]^{3+}$ (+1.28) and $[Eu(\mathbf{L}^{2\prime})(H_2O)]^{3+}$ (+1.29) systems are virtually identical and show that the two complexes do not present important differences in terms of the charge density of the Eu^{III} ion. The evolution of the relative concentration of the species during titration is presented in Figure S13 (Supporting Information), and Figure 7 displays the calculated spectra of the two species, clearly showing that the splitting observed for the $^5D_0 \rightarrow {}^7F_1$ transition is no longer observable in the fluoride adduct. This observation is in excellent agreement with previous work on the replacement of the axial donor in octacoordinated DOTA-type complexes of Eu and Yb,[57] showing that the more polarizable the axial donor, the smaller the splitting. The luminescence lifetime of Eu^{III} was also monitored at 616 nm at the end of the titration. Interestingly, the luminescence lifetime could not be fitted with a simple monoexponential decay, but using a biexponential function led to two components with a short lifetime (τ = 0.52 ms) corresponding to 20% of the total intensity and a long lifetime of 1.20 ms for the other 80%.

It is noteworthy that the short luminescence lifetime corresponds to that observed for the complex in Tris buffer (see above). Thus, one can assume that the second species observed corresponds to the fluoride adduct, for which replacement of the water molecules by F^- decreases the non-radiative deactivations and increases the lifetime. Furthermore, the relative proportions calculated for the two species are in good agreement with those obtained by the fitting of the titration data. Nevertheless, the presence of two distinct lifetimes indicates very slow exchange kinetics between the two species ($k_{ex} < 10^3$ s^{-1}), pointing to a large activation energy necessary for the exchange of water with fluoride.

X-ray Crystal Structures. Crystals of $[La(\mathbf{L}^{2})Cl]Cl_2 \cdot 4H_2O$ were obtained by the slow evaporation of an aqueous solution of the complex. The 2-hydroxyethoxy groups

dx.doi.org/10.1021/ic201447c | Inorg. Chem. 2011, 50, 12508–12521

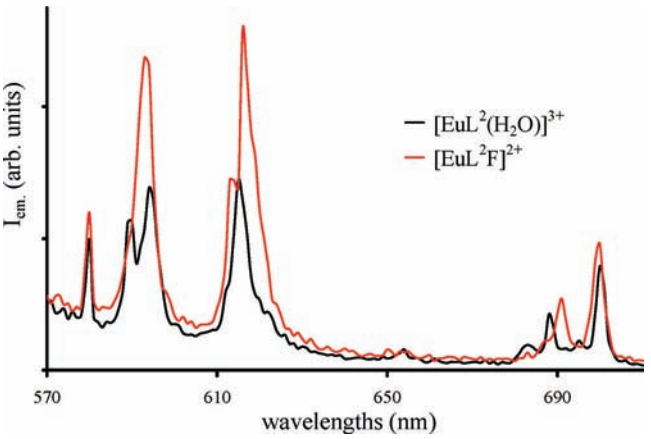

Figure 7. Calculated emission spectra for the species observed during titration of the $[EuL^2(H_2O)]^{3+}$ complex with NaF.

are heavily disordered, which results in large displacement ellipsoids for some of the C and O atoms of the side chains. Crystals also contain heavily disordered water molecules involved in hydrogen-bonding interaction with the Cl^- anions, which, in turn, are hydrogen-bonded to the amide NH groups of the ligand. However, this disorder does not affect the positions in the vicinity of the metal ion. As expected, the La^{III} ion is coordinated to the four N atoms of the cyclen moiety and to the O atoms of the amide pendant arms. Nine-coordination is completed by coordination of a capping chloride anion, which presumably replaces the inner-sphere water molecule coordinating to the metal ion in an aqueous solution. Views of the structure of the $[La(L^2)Cl]^{2+}$ complex are shown in Figure 8, while bond distances of the metal coordination environment are given in Table 2. The $[La(L^2)Cl]^{2+}$ complex possesses a crystallographically imposed C_4 symmetry, which results in four identical La−N and La−O distances. The La1−N1 [2.788(4) Å] and La1−O1 [2.501(3) Å] distances are very similar to those observed in the solid state for the $[La(DOTA)]^-$ complex (2.769 and 2.492 Å, respectively).[58] The La1−Cl1 distance [2.811(3) Å] is close to those observed for other nine-coordinated La^{III} complexes[59] and similar to that observed for a tetrapyridyl DOTA complex of europium [Eu−Cl = 2.763(3) Å], for which the Eu−Cl distance can be tuned in the solid state by changing the noncoordinated anions.[60]

Slow evaporation of an aqueous solution of the Eu^{III} complex of L^1 in the presence of a 4-fold excess of NaF gave single crystals of $[Eu_2(L^1)_2F]Cl_3F_2$ suitable for X-ray diffraction analysis. Crystals contain the $[Eu_2(L^1)_2F]^{5+}$ entity, noncoordinated F^- and Cl^- anions, and heavily disordered water molecules involved in hydrogen-bonding interaction with the anions and the NH groups of the ligand. The 2-hydroxyethoxy groups of the ligand are again heavily disordered, resulting in large displacement ellipsoids for some of the C and O atoms of the side chains. The asymmetric unit contains a half $[Eu_2(L^1)_2F]^{5+}$ unit, with the Eu and F atoms lying on the C_2 axis of the monoclinic space group $P2/n$. Views of the structures of the $[Eu_2(L^1)_2F]^{5+}$ and $[Eu(L^1)F]^{2+}$ entities are shown in Figure 9, while bond distances of the metal coordination environment are given in Table 2.

In $[Eu_2(L^1)_2F]^{5+}$, two $[Eu(L^1)]^{3+}$ units are linked by a bridging fluoride ligand, which results in the formation of an uncommon linear Eu1−F1−Eu2 unit. Indeed, only a few examples of Eu^{III} complexes containing doubly-[61] or triply-,[62] bridging fluoride

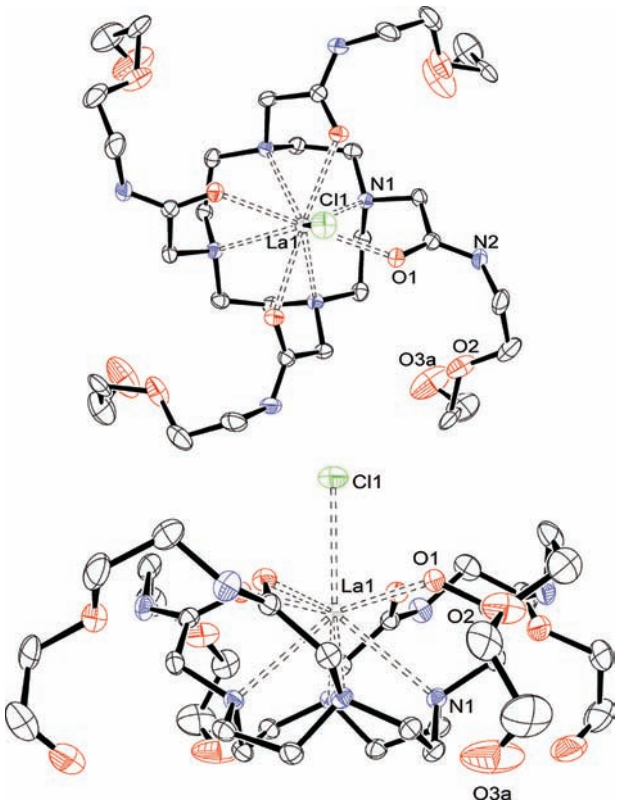

Figure 8. Views of the structure of the $[La(L^2)Cl]^{2+}$ cation along (top) and perpendicular (bottom) to the C_4 axis. The ORTEP plot is at the 30% probability level. H atoms are omitted for the sake of simplicity.

ligands have been reported, where the Eu−F−Eu angles are in the range 95−112°. Concerning the structurally characterized complexes of other Ln^{III} ions containing bridging fluoride ligands, Ln−F−Ln angles in the range 98−179° have been observed.[63] The $[Eu_2(L^1)_2F]^{5+}$ entity appears to be stabilized by the presence of $\pi-\pi$-stacking interactions involving the pyridyl rings of neighboring L^1 units. The mean least-squares planes defined by these aromatic rings intersect at 13.5°, while the distance between their centroids amounts to 3.50 Å. The formation of the $[Eu_2(L^1)_2F]^{5+}$ unit appears to be further assisted by the presence of weak C−H··F hydrogen-bonding interactions involving C−H groups of the pyridyl units [C10···F1 3.103 Å, H10···F1 2.662 Å, C10−H10···F1 108.8°; C60···F1 3.129 Å, H60···F1 2.699 Å, C60−H60···F1 108.3°]. The two metal ions present in the $[Eu_2(L^1)_2F]^{5+}$ unit possess very similar distances to the donor atoms of the ligand. The distances between the metal ions and the N atoms of the macrocycle and the Eu−O distances are both slightly longer than those observed for other Eu^{III}DOTA tetraamide complexes.[64] The distances between the Eu and N atoms of the pyridyl units are, however, ca. 0.05 Å shorter than those observed for $[Eu(L^{py})]^{3+}$.[34]

Both the $[Eu_2(L^1)_2F]^{5+}$ and $[La(L^2)Cl]^{2+}$ complexes crystallize as racemates with a capped SAP coordination polyhedron around the metal ion [$\Lambda(\delta\delta\delta\delta)$ and $\Delta(\lambda\lambda\lambda\lambda)$]. The coordination polyhedra may be considered to be comprised of two nearly parallel planes (0.0 and 3.9° for the complexes of L^1 and L^2, respectively): The four N atoms of cyclen describe the basal plane, while the donor atoms of the pendant arms delineate the upper plane. The coordinated fluoride or chloride anion is capping the

dx.doi.org/10.1021/ic201447c | Inorg. Chem. 2011, 50, 12508–12521

Table 2. Bond Distances (Å) of the Metal Coordination Environments in $[La(L^2)Cl]^{2+}$ and $[Eu_2(L^1)_2F]^{5+}$ (See Figures 8 and 9 for Labeling)

$[La(L^2)Cl]^{2+}$		$[Eu_2(L^1)_2F]^{5+a}$			
La1−N1	2.788(4)	Eu1−F1	2.330(2)	Eu2−F1	2.324(2)
La1−O1	2.501(3)	Eu1−O16	2.421(3)	Eu2−O66	2.410(3)
La1−Cl1	2.811(3)	Eu1−N9	2.545(4)	Eu2−N59	2.555(4)
		Eu1−N1	2.715(4)	Eu2−N51	2.673(4)
		Eu1−N4	2.730(4)	Eu2−N54	2.731(4)

[a]Symmetry transformations used to generate equivalent atoms: $-x + {}^1/_2, y, -z + {}^1/_2$.

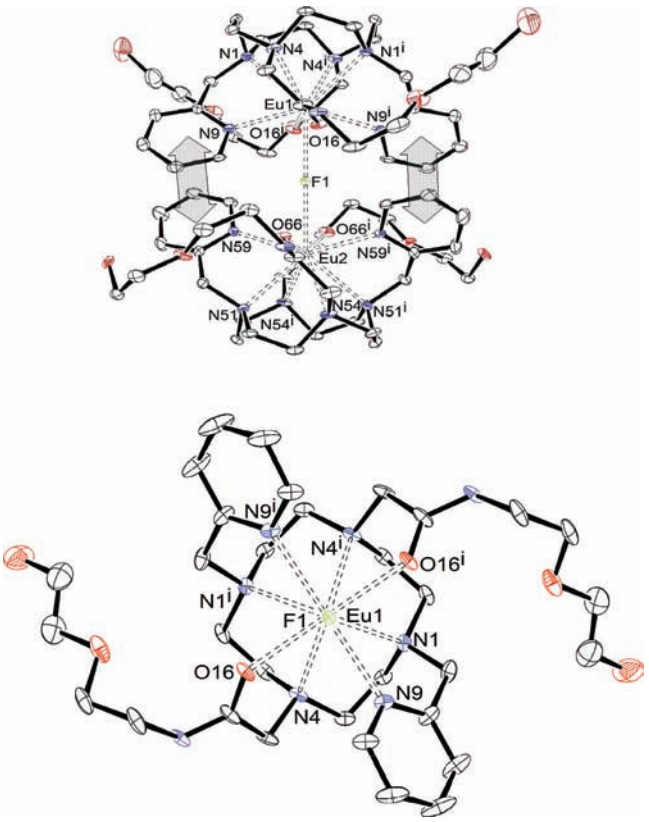

Figure 9. Views of the structure of the $[Eu_2(L^1)_2F]^{5+}$ cation perpendicular to the Ln−F−Ln axis (top, block arrows indicating the $\pi-\pi$-stacking interactions) and of the $[Eu(L^1)F]^{2+}$ complex entity along the Ln−F−Ln axis (bottom). The ORTEP plots are at the 30% probability level. H atoms are omitted for the sake of simplicity.

upper plane. The mean twist angle (Φ) between the upper and lower planes amounts to 37.1° ($[Eu_2(L^1)_2F]^{5+}$) and 37.6° ($[La(L^2)Cl]^{2+}$). These values are very similar to those observed in the solid-state structures of Ln^{III} complexes of DOTA,[65] DOTAM,[66,67] and DTMA[68,69] (Chart 1) with SAP geometries. The coordination geometry observed for $[La(L^2)Cl]^{2+}$ differs from that observed for the $[La(DOTA)]^-$ complex,[58] which adopts a TSAP geometry in the solid state. A TSAP geometry was also observed for the $[Ln(L^{py})]^{3+}$ (Ln = Pr, Nd, or Eu)[34] and $[Ln(DOTAM)(H_2O)]^{3+}$ (Ln = Pr or Eu)[70,71] complexes. However, the geometry adopted by the complexes in the solid state does not necessarily reflect their solution structures because it has been shown that the population of the SAP and TSAP isomers is substantially affected by the solvent.[72]

CONCLUSIONS

The interaction of Ln^{III} complexes with fluoride anions is well documented in the literature and has been mainly studied by luminescence of the lanthanide cations or by ^1H NMR spectroscopy. However, investigations on fluoride sensing using cyclen-based lanthanide complexes are very rare because of the weak interactions between the anionic substrate and the metal center. In this study, as a continuation of our recent work involving tetrafunctionalized cyclen-based ligands (DOTA-like) as metalated macrocyclic receptors, we report a detailed investigation on the Ln^{III} complexes of a previously reported ligand $\mathbf{L^1}$ and of its new analogue $\mathbf{L^2}$ containing four *N*-[2-(2-hydroxyethoxy)ethyl]acetamide pendants. By means of NMR studies, DFT calculations, and spectroscopic measurements, we have highlighted various structural and dynamic properties of the complexes in solution. The X-ray structure of $[La(\mathbf{L^2})Cl]Cl_2$, with its coordinated chloride, demonstrates the suitability of the complex for binding electronegative halogen anions. The interaction of fluoride anions with the positively charged $[Eu(\mathbf{L^2})]^{3+}$ complex was monitored by fluorescence titrations, and the results have unambiguously shown a very weak interaction with the anionic substrate (log K = 1.4) compared to the reported fluoride interaction with $[Eu\mathbf{L^1}]^{3+}$ (log K = 2.9).[35] The X-ray structure of the ternary $[Eu(\mathbf{L^1})F]^{2+}$ complex shows a remarkable $[Eu_2(\mathbf{L^1})_2F]^{5+}$ "sandwich" structure including a perfectly linear Eu−F−Eu bridge stabilized by $\pi-\pi$-stacking interactions of opposite pyridyl units. It also suggests the presence, in the solid state, of C−H···F hydrogen-bonding interactions involving C−H groups of the pyridyl moieties and the anion, which could contribute to the overall stability of the adduct. This supplementary interaction most likely persists in solution, explaining at least, in part, the higher binding affinity toward fluoride of $[Eu(\mathbf{L^1})(H_2O)]^{3+}$ in comparison to $[Eu(\mathbf{L^2})(H_2O)]^{3+}$. The above findings suggest that the presence of the two 2-methylpyridyl pendant arms of $\mathbf{L^1}$ confers supplementary forces, leading to a stronger fluoride binding in the $[Eu(\mathbf{L^1})F]$ adduct. These results represent an important step in our investigations in the field of fluoride sensing in aqueous solution, demonstrating that the binding interaction can be increased by playing with the nature of the coordinating pendant arms of the macrocycle, with the introduction of supplementary hydrogen-bonding donors to stabilize the fluoride anion in its apical position on the Ln^{III} coordination sphere. We are currently pursuing efforts in this direction, by using the well-known tools for selective N-alkylation of the cyclen backbone to design new ligands with improved fluoride binding ability.

dx.doi.org/10.1021/ic201447c | Inorg. Chem. 2011, 50, 12508–12521

EXPERIMENTAL SECTION

Materials and Methods. L^1 was prepared as previously reported.[36] All other reagents were commercially obtained and used without further purification; cyclen was purchased from Chematech (Dijon, France); solvents were dried using standard procedures. IR spectra were measured on a Bruker Vertex 70 FT-IR (ATR) spectrometer. ^{1}H and ^{13}C NMR spectra and 2D COSY, HMQC, and HMBC experiments were run on a Bruker 500 or 300 spectrometer. The ^{1}H NMR spectra were referenced by using the HOD signal at 4.79 ppm, and the pD values of the solutions were calculated from the measured pH* values with the following relationship: pD = pH* + 0.4.[73] Elemental analyses were performed at the "Service Commun d'Analyses" of the University of Strasbourg and at the "Service de Microanalyse ISCN" of the CNRS at Gif Sur Yvette. Mass spectra were run at the "Service Commun d'Analyses" of the University of Strasbourg or at the "Service Commun de Spectrometry de Masse" of the University of Brest.

Syntheses. *2-Bromo-N-[2-(2-hydroxyethoxy)ethyl]acetamide (1).* This compound was synthesized as previously described[36] and purified by an additional chromatography on SiO_2 (R_f = 0.38 in ethyl acetate) with a $CHCl_3$/ethyl acetate 0 → 30% mixture as the eluent to give 1.9 g of **1** as a colorless oil (yield 62%). Elem anal. Calcd for $C_6H_{12}BrNO_3$: C, 31.88; H, 5.35; N, 6.20. Found: C, 31.57; H, 5.51; N, 5.94. ^{1}H NMR ($CDCl_3$, 400.13 MHz, 25 °C, TMS): δ 2.88 (q, 2H, $-CH_2NH$), 3.04 (t, 2H, $-CH_2CH_2O$), 3.16 (t, 2H, $-CH_2CH_2NH$), 3.40 (t, 2H, $-CH_2OH$), 3.96 (s, 2H, $-CH_2Br$), 7.59 (s, 1H, NH). ^{13}C NMR ($CDCl_3$, 100.62 MHz, 25 °C, TMS): δ 278.3 ($-CH_2Br$), 39.3 ($-CH_2NH$), 60.5 ($-CH_2OH$), 68.4 ($-CH_2CH_2NH$), 71.5 ($-CH_2CH_2OH$), 166.7 (CO). ESI-HRMS in $CHCl_3$: m/z 226.0075 ($[M + H]^+$). IR (ATR, cm^{-1}): ν 3277 (br, OH), 1651 (NHC═O), 573 (CBr).

2-[2-(2-Chloroacetamido)ethoxy]ethyl Propionate (2). A solution of propionyl chloride (2.02 g, 20.7 mmol) in anhydrous CH_2Cl_2 (15 mL) was added dropwise to a solution of compound **1** (4.68 g, 20.7 mmol) and freshly distilled pyridine (1.73 g, 20.7 mmol) in the same solvent (15 mL). The mixture was stirred overnight, and then 10 mL of water was added. The aqueous solution was extracted with CH_2Cl_2 (3 × 60 mL). The combined organic extracts were dried over $MgSO_4$, and the solvent was evaporated. The residue was purified on SiO_2 (R_f = 0.34 in 3:1 petroleum ether/$CHCl_3$) with a petroleum ether/$CHCl_3$ 0 → 50% mixture as the eluent to give 4.22 g of **2** as a colorless oil (yield 78%). Elem anal. Calcd for $C_9H_{16}ClNO_4{\cdot}0.2CHCl_3$: C, 42.25; H, 6.24; N, 5.36. Found: C, 42.30; H, 6.39; N, 5.33. ^{1}H NMR ($CDCl_3$, 400.13 MHz, 25 °C, TMS): δ 1.09 (t, 3H, CH_3), 2.31 (q, 2H, $-CH_2CH_3$), 3.47 (t, 2H, $-CH_2NH$), 3.58 (t, 2H, $-CH_2CH_2NH$), 3.65 (t, 2H, CH_2O), 4.04 (t, 2H, CH_2OCO), 4.28 (s, 2H, CH_2Cl), 6.88 (1H, NH). ^{13}C NMR ($CDCl_3$, 100.62 MHz, 25 °C, TMS): δ 9.3 (CH_3), 26.8 (CH_2CO), 38.2 (CH_2NH), 42.0 (CH_2Cl), 62.6 (CH_2OCO), 67.8 (CH_2O), 68.3 (OCH_2), 165.8 (NHCO), 173.7 (CO). ESI-HRMS in $CHCl_3$: m/z260.06594 ($[M + Na]^+$). IR (ATR, cm^{-1}): ν 1732 (OC═O), 1659 (NHC═O), 806 (CCl).

[[[[2,2′,2″,2‴-(1,4,7,10-Tetraazacyclododecanyl-1,4,7,10-tetrayl)-tetrakis(acetyl)]tetrakis(azanediyl)]tetrakis(ethane-2,1-diyl)]-tetrakis(oxy)]tetrakis(ethane-2,1-diyl) Tetrapropionate (3). A solution of compound **2** (2.95 g, 11.94 mmol) and NaI (1.79 g, 11.94 mmol) in dry CH_3CN (15 mL) was added to a solution of cyclen (0.45 g, 2.84 mmol) in the same solvent (15 mL). The reaction mixture was stirred at room temperature in the presence of anhydrous K_2CO_3 (1.65 g, 11.94 mmol) for 3 days. The mixture was filtered to remove excess K_2CO_3 and the solvent evaporated. Water (15 mL) was added, and the resulting mixture was extracted with $CHCl_3$ (3 × 50 mL). The combined organic extracts were dried over $MgSO_4$, and the solvent was evaporated. The crude product was purified by column chromatography on SiO_2 (R_f = 0.18 in $CHCl_3$) with a $CHCl_2$/MeOH 2% mixture as the eluent to give 1.9 g of **2** as a dark-brown oil (yield 67%). Elem anal. Calcd for $C_{44}H_{80}N_8O_{16}{\cdot}2CHCl_3$: C, 45.44; H, 6.80; N, 9.22. Found: C, 45.15; H, 7.08; N, 9.02. ^{1}H NMR ($CDCl_3$, 400.13 MHz, 25 °C, TMS): δ 1.16 (t, 12H, CH_3), 1.49 (q, 8H, CH_2CH_3), 2.30 (m, 16H, CH_2N), 3.05 (s, 8H, CH_2CO), 3.42 (t, 8H, CH_2NH), 3.49 (t, 8H, $NHCH_2$), 3.55 (t, 8H, CH_2CH_2O), 4.24 (t, 8H, CH_2O), 7.82 (s, 4H, NH). ^{13}C NMR ($CDCl_3$, 100.62 MHz, 25 °C, TMS): δ 8.8 ($-CH_3$), 27.1 (CH_2CH_3), 38.7 (CH_2NH), 51.6 (NCH_2), 62.9 (CH_2CO), 65.4 (CH_2O), 68.6 (CH_2OCO), 69.1 (CH_2O), 174.0 (NHCO), 174.1 (OCO). ESI-HRMS in $CHCl_3$: m/z 429.29192 ($[M + 2H]^{2+}/2$), 977.29192 ($[M + H]^+$). IR (ATR, cm^{-1}): ν 1732 (OC═O), 1659 (NHC═O).

2,2′,2″,2‴-(1,4,7,10-Tetraazacyclododecane-1,4,7,10-tetrayl)-tetrakis[N-[2-(2-hydroxyethoxy)ethyl]acetamide] (L^2). Compound **3** (1.0 g, 1.02 mmol) was dissolved in 2 M HCl (10 mL) and the solution stirred for 12 h. The mixture was neutralized with a 2 M NaOH solution and then concentrated to 5 mL. The aqueous solution was extracted with CH_2Cl_2 (3 × 20 mL), and the combined organic extracts were dried over Mg_2SO_4. Evaporation of the solvent gave 0.60 g of L^2 as a white solid (yield 78%; mp = 156 °C). Elem anal. Calcd for $C_{32}H_{64}N_8O_{12}{\cdot}2H_2O$: C, 48.72; H, 8.69; N, 14.20. Found: C, 48.39; H, 8.70; N, 14.11. ^{1}H NMR ($CDCl_3$, 400.13 MHz, 25 °C, TMS): δ 2.29 (m, 16H, CH_2N), 2.77 (s, 4H, OH), 3.06 (s, 8H, CH_2CO), 3.32 (t, 8H, CH_2NH), 3.71 (m, 16H, CH_2O), 3.80 (t, 8H, CH_2OH), 8.04 (s, 4H, NH). ^{13}C NMR ($CDCl_3$, 100.62 MHz, 25 °C, TMS): δ 41.9 ($-CH_2NH$), 53.3 (NCH_2), 60.0 (CH_2CO), 63.4 (CH_2OH), 71.9 ($NHCH_2CH_2$), 74.6 (OCH_2), 176.3 (CO). ^{1}H NMR (D_2O, 400.13 MHz, 25 °C, TMS): δ 2.95 (m, 8H, CH_2N), 3.32 (m, 8H, CH_2N), 3.77 (m, 16H, CH_2CO, CH_2NH), 3.96 (m, 24H, CH_2O, CH_2OH). ^{13}C NMR (D_2O, 100.62 MHz, 25 °C, TMS): δ 39.4 ($-CH_2NH$), 51.1 (NCH_2), 57.1 (CH_2CO), 60.4 (CH_2OH), 68.6 ($NHCH_2CH_2$), 71.6 (OCH_2), 173.2 (CO). ESI-HRMS in $CHCl_3$: m/z 377.23940 ($[M + 2H]^{2+}/2$). MALDI-TOF in $CHCl_3$/dithranol: m/z 753.498 ($[M + H]^+$), 775.480 ($[M + Na]^+$). IR (ATR, cm^{-1}): ν 3280 (OH), 1652 (NHC═O).

Lanthanide Complexes: General Procedure. To a solution of the ligand (0.05−0.10 mmol) in methanol (5 mL) was added 1 equiv of the corresponding lanthanide chloride dissolved in methanol (5 mL). The solution was stirred for 3 h at 45 °C. The solution was then concentrated to ca. 2 mL, and the addition of Et_2O resulted in precipitation of the complex, which was isolated by centrifugation. After treatment with Et_2O and drying under vacuum, the complexes were obtained as highly hygroscopic yellow solids.

[Tb(L^2)(H_2O)]Cl_3. General procedure from L^2 (38 mg, 0.050 mmol) and $TbCl_3{\cdot}6H_2O$ (13.5 mg, 0.050 mmol). Yield: 40 mg (79%). IR (cm^{-1}, ATR): ν 3228 (w, br), 3092 (w), 2942 (w), 2871 (w), 2160 (w), 2028 (w), 1977 (w), 1626 (s), 1588 (s, br), 1366 (m), 1299 (m), 1247 (m), 1118 (s), 1065 (s). ESI$^+$-MS (H_2O): m/z 981.4 ($[Tb(L^2)Cl_2]^+$, 6%), 858.3 ($[Tb(L^2)Cl(C_4H_9O_2)]^+$, 17%), 822.3 ($[Tb(L^2)(C_4H_9O_2)]^+$, 13%), 473.2 ($[Tb(L^2)Cl]^{2+}$, 100%), 411.7 ($[Tb(L^2)(C_4H_9O_2)]^{2+}$, 100%). Elem anal. Calcd for $C_{32}H_{64}N_8O_{12}TbCl_3{\cdot}5NaCl{\cdot}3H_2O$: C, 28.17; H, 5.17; N, 8.21. Found: C, 28.08; H, 5.32; N, 7.95.

[Eu(L^2)(H_2O)]Cl_3. General procedure from L^2 (39 mg, 0.052 mmol) and $EuCl_3{\cdot}6H_2O$ (13.5 mg, 0.052 mmol). Yield: 44 mg (84%). IR (cm^{-1}, ATR): ν 3240 (w, br), 3091 (w), 2940 (w), 2868 (w), 2159 (w), 2028 (w), 1977 (w), 1713 (w), 1620 (s), 1582 (s, br), 1460 (m), 1389 (m), 1365 (m), 1293 (m), 1244 (m), 1118 (s), 1062 (s). ESI$^+$-MS (H_2O): m/z 973.3 ($[Eu(L^2)Cl_2]^+$, 5%), 852.3 ($[Eu(L^2)Cl(C_4H_9O_2H)]^+$, 22%), 753.5 ($[L^2]$, 68%), 470.2 ($[Eu(L^2)Cl]^{2+}$, 70%), 408.6 ($[Eu(L^2)(C_4H_9O_2)]^{2+}$, 100%). Anal. Calcd for $C_{32}H_{64}N_8O_{12}EuCl_3{\cdot}4NaCl{\cdot}3H_2O$: C, 29.58; H, 5.43; N, 8.62. Found: C, 29.51; H, 5.44; N, 8.32.

[La(L^2)(H_2O)]Cl_3. General procedure from L^2 (51 mg, 0.068 mmol) and $LaCl_3{\cdot}7H_2O$ (25 mg, 0.068 mmol). Yield: 57 mg (84%). MALDI-TOF/MS (H_2O): m/z 889.4 ($[LaL^3(2H)]^+$, 100%), 802.3 ($[LaL^3(C_4H_9O_2H)]^+$, 18%).

Yb(L^2)(H_2O)]Cl_3. General procedure from L^2 (45 mg, 0.060 mmol) and $YbCl_3{\cdot}6H_2O$ (23 mg, 0.06 mmol). Yield: 57 mg (90%). MALDI-TOF/MS (H_2O): m/z 924.4 ($[Yb(L^2)(2H)]^+$, 100%), 837.3 ($[YbL^3(C_4H_9O_2H)]^+$, 50%).

Yb(L^1)(H_2O)]Cl_3. General procedure from L^1 (70 mg, 0.109 mmol) and $YbCl_3{\cdot}6H_2O$ (39 mg, 0.109 mmol). Yield: 78 mg (76%). MALDI-TOF/MS (H_2O): m/z 816.3 ($[Yb(L^1)(2H)]^+$, 100%), 729.3 ($[Yb(L^1)(C_4H_9O_2H)]^+$, 43%).

dx.doi.org/10.1021/ic201447c | Inorg. Chem. 2011, 50, 12508–12521

Lu(L²)(H₂O)]Cl₃. General procedure from $\mathbf{L^2}$ (86 mg, 0.114 mmol) and $LuCl_3 \cdot 6H_2O$ (38 mg, 0.098 mmol). Yield: 102 mg (85%). MALDI-TOF/MS (H_2O): *m/z* 925.4 ($[Lu(\mathbf{L^2})(2H)]^+$, 100%), 838.3 ($[Lu(\mathbf{L^2})(C_4H_9O_2H)]^+$, 44%).

Lu(L¹)(H₂O)]Cl₃. General procedure from $\mathbf{L^1}$ (63 mg, 0.098 mmol) and $LuCl_3 \cdot 6H_2O$ (44 mg, 0.114 mmol). Yield: 83 mg (90%). MALDI-TOF/MS (H_2O): *m/z* 730.3 ($[Lu(\mathbf{L^1})(C_4H_9O_2H)]^+$, 100%).

Single-Crystal X-ray Diffraction Measurements. Suitable single crystals for X-ray diffraction determination of $[La(\mathbf{L^2})Cl]Cl_2 \cdot 4H_2O$ were obtained by the slow evaporation of an aqueous solution of the synthesized complex. Three-dimensional X-ray diffraction data were collected on an X-CALIBUR-2 CCD 4-circle diffractometer (Oxford Diffraction; reference number CCDC 832493). Data reduction, including interframe scaling, Lorentz, polarization, empirical absorption, and detector sensitivity corrections, was carried out using attached programs of *Crysalis* software[74] (Oxford Diffraction). Complex scattering factors were taken from the program *SHELX97*[75] running under the *WinGX* program system,[76] as implemented on a Pentium computer. The structure was solved by direct methods with *SHELXS-97* and refined[75] by full-matrix least squares on F^2. All H atoms were included in calculated positions and refined in the riding mode, except the H atom bonded to O3C and those of the water molecules, which were located in a difference electron-density map, and the positional parameters were fixed. However, it was not possible to locate one of the H atoms bonded to O2w. The long side chains of the ligand molecule present conformational disorder that has been modeled in two locations (except for the terminal OH moiety, for which three alternative positions were located), and the corresponding atom site occupations were refined. The final value for the population parameters was 46(2)% for the positions labeled as A and the complementary one, 54(2)%, for the atoms labeled as B. For the terminal O atoms, the population parameters were refined with the SUMP instruction and the final population values achieved were 45(1)% for O3A, 19(1)% for O3B, and 35(1)% for O3C. Refinement converged with anisotropic displacement parameters for all non-H atoms after imposing 116 restraints. Crystal data and details on data collection and refinement are summarized in Table 3.

For $[Eu_2(\mathbf{L^1})_2F]F_2Cl_3$, three-dimensional X-ray diffraction data were collected on a Bruker X8 Kappa APEX II CCD (reference number CCDC 832492). Data were corrected for Lorentz and polarization effects and for absorption by semiempirical methods[77] based on symmetry-equivalent reflections. The crystal symmetry corresponds to the monoclinic crystal system, although the β angle is very close to 90° and the R_{int} value is very low for the orthorhombic crystal classes. All of the screened crystals were twinned by pseudomerohedry,[78] with the twin operator being a 2-fold axis perpendicular to the monoclinic 2-fold of the true 2/*m* crystal class. The twin domain ratio is close to 50:50, and this is the reason why the structure appears to belong to a higher-symmetry crystal system (orthorhombic) instead of the true monoclinic one. Table 3 shows the details for the twin operator definition and domain populations. Complex scattering factors were taken from the program *SHELX97*[75] running under the *WinGX* program system,[75] as implemented on a Pentium computer. The structure was solved by direct methods with *SIR-97*[79] and refined[75] by full-matrix least squares on F^2. All H atoms were included in calculated positions and refined in the riding mode. No H atoms could be located for water molecules. The long side chains of the ligand molecule present conformational disorder that has been modeled in two locations, and the corresponding atom site occupations were refined. The final value for the population parameter is 57.8(3)% for the positions labeled as A and the complementary one, 42.2(3)%, for the atoms labeled as B. Most of the Cl^- and F^- counterions, together with the water solvent molecules, are also disordered in two mutually exclusive locations. Because of the high degree of disorder displayed by the structure, 806 restraints of several types have been used on displacement parameters (DELU, SIMU, and ISOR) to optimize convergence of the refinement procedure performed with the *SHELXL* program.[75] Crystal data and details on data collection and refinement are summarized in Table 3.

Spectroscopic Measurements. UV−vis absorption spectra were recorded on a Specord 205 (Analytik Jena) spectrometer. Steady-state emission and excitation spectra were recorded on a Horiba Jobin Yvon Fluorolog 3 spectrometer working with a continuous 450 W Xe lamp. Detection was performed with a Hamamatsu R928 photomultiplier. All spectra were corrected for instrumental functions. When necessary, a 370 nm cutoff filter was used to eliminate the second-order artifacts. The ligand emission lifetime in an EtOH solution was measured in time-resolved mode, by monitoring the decay at the maximum of the emission spectrum using a Jobin Yvon FluoroHub single-photon-counting controller, fitted with a 303 nm Jobin Yvon NanoLED. The decays were analyzed with DataStation v2.4. The Eu and Tb complexes of $\mathbf{L^2}$ were purified prior to measurements, on reverse-phase C18 chromatographic columns (Polygoprep 60-50, Macherey Nagel, Düren, Germany) using a 100:0 to 90:10 water/MeOH gradient.

Table 3. Crystal Data and Refinement Details for $[La(\mathbf{L^2})Cl]Cl_2 \cdot 4H_2O$ and $[Eu_2(\mathbf{L^1})_2F]F_2Cl_3$

	$[La(\mathbf{L^2})Cl]Cl_2 \cdot 4H_2O$	$[Eu_2(\mathbf{L^1})_2F]F_2Cl_3$
formula	$C_{32}H_{71}Cl_3LaN_8O_{16}$	$C_{64}H_{104}Cl_3Eu_2F_3N_{16}O_{30.16}$
MW	1069.23	2047.45
cryst syst	tetragonal	monoclinic
space group	*P*4/*ncc*	*P*2/*n*
T/K	170(2)	100(2)
a/Å	14.2869(4)	13.3092(3)
b/Å	14.2869(4)	16.5654(3)
c/Å	23.9665(11)	20.9868(4)
α/deg	90	90
β/deg	90	90.018(1)
γ/deg	90	90
V/Å³	4891.9(3)	4627.01(16)
F(000)	2220	2090.4
Z	4	2
λ(Mo Kα), Å	0.710 73	0.710 73
D_{calc}/g cm^{-3}	1.452	1.470
μ/mm^{-1}	1.106	1.516
θ range/deg	2.85−26.37	0.97−29.39
R_{int}	0.0767	0.0675
reflns measd	34 445	84 946
unique reflns	2507	12 766
reflns obsd	1519	9325
GOF on F^2	1.134	1.021
twin law		1, 0, 0/0, −1, 0/0, 0, −1
twin domain fraction/%		45.6(1)
R1[a]	0.0446	0.0417
wR2 (all data)[b]	0.1381	0.1117
largest differences in peak and hole/e Å^{-3}	0.908 and −0.452	1.656 and −0.794

[a] $R1 = \sum||F_o| - |F_c||/\sum|F_o|$. [b] $wR2 = \{\sum[w(|F_o|^2 - |F_c|^2)^2]/\sum[w(F_o^4)]\}^{1/2}$.

Computational Methods. All calculations were performed by employing hybrid DFT with the B3LYP exchange-correlation functional[80,81] and the *Gaussian 09* package (revision A.02).[82] Different computational studies on Ln^{III} complexes have shown that the 4f orbitals do not participate in bonding because of their contraction into the core.[83] As a consequence, no effect of the spin−orbit coupling on the equilibrium geometries of Ln^{III} complexes was found.[84] Thus, spin−orbit effects were not taken into account in the present work. Relativistic effects were considered through the use of relativistic ECPs (RECPs). For computational simplicity in our calculations, the 2-(2-hydroxyethoxy)ethyl chains of ligands $\mathbf{L^1}$ and $\mathbf{L^2}$ were substituted by methyl groups, with the methyl-substituted ligands being denoted as $\mathbf{L^{1'}}$ and $\mathbf{L^{2'}}$. Full geometry optimizations of the $[Ln(\mathbf{L^{1'}})(H_2O)]^{3+}$ (Ln = Yb or Lu) and $[Ln(\mathbf{L^{2'}})(H_2O)]^{3+}$ (Ln = La, Eu, Yb, or Lu) systems were performed in vacuo by using the

RECP of Dolg et al.[50] and the related [5s4p3d] GTO valence basis set for the lanthanides and the 6-31G(d) basis set for C, H, N, and O atoms. No symmetry constraints have been imposed during optimization. The default values for the integration grid ("fine") and the self-consistent-field energy convergence criteria (10^{-6}) were used. The stationary points found on the potential energy surfaces as a result of the geometry optimizations have been tested to represent energy minima rather than saddle points via frequency analysis. The ring-inversion and arm-rotation processes in $[Lu(\mathbf{L^2})(H_2O)]^{3+}$ were investigated by means of the synchronous transit-guided quasi-Newton method.[85] The nature of the saddle points and intermediates was characterized by frequency analysis. The free-energy barriers include nonpotential energy contributions (that is, zero-point energies and thermal terms) obtained by frequency analysis.

■ ASSOCIATED CONTENT

Ⓢ Supporting Information

X-ray crystallographic files in CIF format, ^1H and ^{13}C NMR spectral data, calculated geometrical parameters (B3LYP) of the two isomers of $[Ln(\mathbf{L^{1'}})(H_2O)]^{3+}$ and $[Ln(\mathbf{L^{2'}})(H_2O)]^{3+}$ complexes, ESI$^+$-MS, ^1H NMR spectra of $[Lu(\mathbf{L^1})(H_2O)]^{3+}$ and $[Lu(\mathbf{L^2})(H_2O)]^{3+}$, Eyring plot for $[Lu(\mathbf{L^2})(H_2O)]^{3+}$, species distribution diagram for $[Lu(\mathbf{L^2})(H_2O)]^{3+}$ as a function of the F^- concentration, and optimized Cartesian coordinates (B3LYP) for the $[Ln(\mathbf{L^{1'}})(H_2O)]^{3+}$ (Ln = Yb or Lu) and $[Ln(\mathbf{L^{2'}})(H_2O)]^{3+}$ (Ln = La, Eu, Yb, or Lu) systems. This material is available free of charge via the Internet at http://pubs.acs.org.

■ AUTHOR INFORMATION

Corresponding Author

*E-mail: L.charbonn@unistra.fr (L.J.C.), cplatas@udc.es (C.P.-I.), raphael.tripier@univ-brest.fr (R.T.).

■ ACKNOWLEDGMENTS

The authors are indebted to Centro de Supercomputación de Galicia for providing the computer facilities. L.M.P.Lima and R.T. acknowledge financial support from the IFR 148 ScInBioS and of the Conseil General du Finistère. The authors gratefully acknowledge Antonio L. Llamas-Saiz (Unidade de Raios X, RIAIDT, Universidade de Santiago de Compostela, Spain) for his assistance with the resolution of the X-ray crystal structures.

■ REFERENCES

(1) Ayoob, S.; Gubta, A. K. *Crit. Rev. Environ. Sci. Technol.* **2006**, *36*, 433−487.
(2) Aaseth, J.; Shimshi, M.; Gabrilove, J. L.; Birketvedt, G. S. *J. Trace Elements Med. Biol.* **2004**, *17*, 83−92.
(3) Ametamey, S. M.; Honer, M.; Schubiger, P. A. *Chem. Rev.* **2008**, *108*, 1501−1516.
(4) Cerklewski, F. L. *Nutr. Res. (N.Y.)* **1997**, *5*, 907−927.
(5) (a) Connet, P. *Fluoride* **2007**, *40*, 155−158. (b) Foulkes, R. G. *Fluoride* **2007**, *40*, 229−237. (c) Yu., Y.; Yang, W.; Dong, Z.; Wan, C.; Zhang, J.; Liu, J.; Xiao, K.; Huang, Y.; Lu, B. *Fluoride* **2008**, *41*, 134−138. (d) Ozsvath, D. L. *Rev. Environ. Sci. Biotechnol.* **2009**, *8*, 59−79. (e) Ozsvath, D. L. *Rev. Environ. Sci. Biotechnol.* **2009**, *8*, 59−79.
(6) (a) Larsson, L. *Acta Chem. Scand.* **1957**, *11*, 1131−1142. (b) Zhang, S.-W.; Swager, T. M. *J. Am. Chem. Soc.* **2003**, *125*, 3420−3421.
(7) (a) Costero, A. M.; Bañuls, M. J.; Burell, M. J.; Ward, M. D.; Argent, S. *Tetrahedron* **2004**, *60*, 9471−9478. (b) Kang, S. O.; Begur, R. A.; Bowman-James, K. *Angew. Chem., Int. Ed.* **2006**, *45*, 7882−7894. (c) Kang, S. O.; Powell, D.; Bowman-James, K. *J. Am. Chem. Soc.* **2005**, *127*, 13478−13479.
(8) Chen, C.-F.; Chen, Q.-Y. *Tetrahedron Lett.* **2004**, *45*, 3957−3960.
(9) Bates, G. W.; Gale, P. A.; Light, M. E. *Chem. Commun.* **2007**, 2121−2123.
(10) An, B.-K.; Wang, X.; Burn, P. L.; Meredith, P. *ChemPhysChem* **2010**, *11*, 3517−3521.
(11) (a) Pérez-Ruíz, R.; Díaz, Y.; Goldfuss, B.; Hertel, D.; Meerholz, K.; Griesbeck, A. G. *Org. Biomol. Chem.* **2009**, *7*, 3499−3504. (b) Vázquez, M.; Fabbrizzi, L.; Taglietti, A.; Pedrido, R. M.; González-Noya, A. M.; Bermejo, M. R. *Angew. Chem., Int. Ed.* **2004**, *43*, 1962−1965. (c) Xu, G.; Tarr, M. A. *Chem. Commun.* **2004**, 1050−1051. (d) Lee, J. Y.; Cho, E. J.; Mukamel, S.; Nam, K. C. *J. Org. Chem.* **2004**, *69*, 943−950.
(12) (a) Camiolo, S.; Gale, P. A. *Chem. Commun.* **2000**, 1129−1130. (b) Cafeo, G.; Kohnke, F. H.; White, A. J. P.; Garozzo, D.; Messina, A. *Chem.—Eur. J.* **2007**, *13*, 649−656. (c) Denekamp, C.; Suwinska, K.; Salman, H.; Abraham, Y.; Eichen, Y.; Ari, J. B. *Chem.—Eur. J.* **2007**, *13*, 657−665. (d) Woods, C. J.; Camiolo, S.; Light, M. E.; Coles, S. J.; Hursthouse, M. B.; King, M. A.; Gale, P. A.; Essex, J. W. *J. Am. Chem. Soc.* **2002**, *124*, 8644−8652.
(13) Lu, Q.-S.; Dong, L.; Zhang, J.; Li, J.; Jiang, L.; Huang, Y.; Qin, S.; Hu, C.-W.; Yu, X.-Q. *Org. Lett.* **2009**, *11*, 669−672.
(14) Hossain, M. A.; Kang, S. O.; Powell, D.; Bowman-James, K. *Inorg. Chem.* **2003**, *42*, 1397−1399.
(15) Guha, S.; Saha, S. *J. Am. Chem. Soc.* **2010**, *132*, 17674−17677.
(16) (a) Yamaguchi, S.; Akiyama, S.; Tamao, K. *J. Am. Chem. Soc.* **2001**, *123*, 11372−11375. (b) Solé, S.; Gavia, F. P. *Chem. Commun.* **2004**, 1284−1285. (c) Hudnall, T. W.; Chiu, C.-W.; Gabbai, F. P. *Acc. Chem. Res.* **2009**, *42*, 388−397. (d) Wade, C. R.; Broomsgrove, A. E. J.; Aldridge, S.; Gabbai, F. P. *Chem. Rev.* **2010**, *110*, 3958−3984.
(17) Kim, Y.; Gabbai, P. *J. Am. Chem. Soc.* **2009**, *131*, 3363−3369.
(18) Lehaire, M.-L.; Scopelliti, R.; Piotrowski, H.; Severin, K. *Angew. Chem., Int. Ed.* **2002**, *41*, 1419−1422.
(19) Ambrosi, G.; Formica, M.; Fusi, V.; Giorgi, L.; Guerra, A.; Micheloni, M.; Paoli, P.; Pontellini, R.; Rossi, P. *Chem.—Eur. J.* **2007**, *13*, 702−712.
(20) Melaimi, M.; Gavia, F. P. *J. Am. Chem. Soc.* **2005**, *127*, 9680−9681.
(21) Badr, I. H.; Meyerhoff, M. E. *J. Am. Chem. Soc.* **2005**, *127*, 5318−5319.
(22) Cametti, M.; Cort, A. D.; Mandolina, L.; Nissinen, M.; Rissanen, K. *New J. Chem.* **2008**, *32*, 1113−1116.
(23) Pearson, R. G. *J. Am. Chem. Soc.* **1963**, *85*, 3533−3539.
(24) For reviews on anion sensing with lanthanide complexes, see: (a) Parker, D. *Coord. Chem. Rev.* **2000**, *205*, 109−130. (b) Tsukube, H.; Shinoda, S. *Chem. Rev.* **2002**, *102*, 2389−2403. (c) Lima, L. M. P.; Tripier, R. *Curr. Inorg. Chem.* **2011**, *1*, 36−60.
(25) For example, see: (a) Tsukube, H.; Suzuki, Y.; Paul, D.; Kataoka, Y.; Shinoda, S. *Chem. Commun.* **2007**, 2533−2535. (b) Best, M. D.; Anslyn, E. V. *Chem.—Eur. J.* **2003**, *9*, 51−57. (c) Charbonnière, L. J.; Schurhammer, R.; Mameri, S.; Wippf, G.; Ziessel, R. F. *Inorg. Chem.* **2005**, *44*, 7151−7160. (d) Schäferling, M.; Wolbeis, O. S. *Chem.—Eur. J.* **2007**, *13*, 4342−4349. (e) Prodi, L.; Montalti, M.; Zaccheroni, N.; Pickaert, G.; Charbonnière, L. J.; Ziessel, R. *New J. Chem.* **2003**, *27*, 134−139.
(26) (a) Yamada, T.; Shinoda, S.; Tsukube, H. *Chem. Commun.* **2002**, 1218−1219. (b) Woods, M.; Sherry, A. D. *Inorg. Chem.* **2003**, *42*, 4401−4408. (c) Bretonnière, Y.; Cann, M. J.; Parker, D.; Slater, R. *Org. Biomol. Chem.* **2004**, *2*, 1624−1632. (d) Atkinson, P.; Murray, B. S.; Parker, D. *Org. Biomol. Chem.* **2006**, *4*, 3166−3171. (e) Blair, S.; Lowe, M. P.; Mathieu, C. E.; Parker, D.; Senanayake, P. K.; Kataky, R. *Inorg. Chem.* **2001**, *40*, 5860−5867.
(27) (a) Tremblay, M. S.; Zhu, Q.; Marti, A. A.; Dyer, J.; Halim, M.; Jokusch, S.; Turro, N. J.; Sames, D. *Org. Lett.* **2006**, *8*, 2723−2726. (b) Charbonnière, L. J.; Mameri, S.; Kadjane, P.; Platas-Iglesias, C.; Ziessel, R. *Inorg. Chem.* **2008**, *47*, 3748−3752. (c) Mameri, S.; Charbonnière, L. J.; Ziessel, R. Z. *Inorg. Chem.* **2004**, *43*, 1819−1821.
(28) (a) Govenlock, L. J.; Mathieu, C. E.; Maupin, C. L.; Parker, D.; Riehl, J. P.; Siligardi, J.; Williams, J. A. G. *Chem. Commun.* **1999**, 1699−1700. (b) Tamiaki, H.; Unno, S.; Takeuchi, E.; Tameshige, N.; Shinoda, S.; Tsukube, H. *Tetrahedron* **2003**, *59*, 10477−10483.

(29) (a) Atkinson, P.; Bretonnière, Y.; Parker, D.; Müller, G. *Helv. Chim. Acta* **2005**, *88*, 391−405. (b) Gunnlaugsonn, T.; Leonard, J. P. *Chem. Commun.* **2005**, 3114−3131. (c) Dickins, R. S.; Aime, S.; Batsanov, A. S.; Beeby, A.; Botta, M.; Bruce, J. I.; Howard, J. A. K.; Love, C. S.; Parker, D.; Peacock, R. D.; Puschmann, H. *J. Am. Chem. Soc.* **2002**, *124*, 12697−12705.
(30) (a) Kataoka, Y.; Dharam, P.; Miyake, H.; Shinoda, S.; Tsukube, H. *Dalton Trans.* **2007**, 2784−2791. (b) Charbonnière, L. J.; Ziessel, R.; Montalti, M.; Zaccheroni, N.; Boehme, C.; Wipff, G. *J. Am. Chem. Soc.* **2002**, *124*, 7779−7788. (c) Dos Santos, C. M. G.; Gunnlaugsson, T. *Dalton Trans.* **2009**, 4712−4721.
(31) (a) Sabbatini, N.; Perathoner, S.; Lattanzi, G.; Dellonte, S.; Balzani, V. *J. Phys. Chem.* **1987**, *91*, 6136−6139. (b) Cross, J. P.; Dadabhoy, A.; Sammes, P. G. *J. Lumin.* **2004**, *110*, 113−124.
(32) (a) Delgado, R.; Félix, V.; Lima, L. M. P.; Price, D. W. *Dalton Trans.* **2007**, 2734−2745. (b) Hermann, P.; Kotek, J.; Kubicek, V.; Lukes, I. *Dalton Trans.* **2008**, 3027−3047.
(33) Montgomery, C. P.; Murria, B. S.; New, E. J.; Pal, R.; Parker, D. *Acc. Chem. Res.* **2009**, *42*, 925−937.
(34) Natrajan, L. S.; Khoabane, N. M.; Dadds, B. L.; Muryn, C. A.; Pritchard, R. G.; Heath, S. L.; Kenwright, A. M.; Kuprov, I.; Faulkner, S. *Inorg. Chem.* **2010**, *49*, 7700−7709.
(35) Tripier, R.; Platas-Iglesias, C.; Boos, A.; Morfin, J.-F.; Charbonnière, L. *Eur. J. Inorg. Chem.* **2010**, 2735−2745.
(36) Morfin, J.-F.; Tripier, R.; Le Baccon, M.; Handel, H. *Polyhedron* **2009**, *28*, 3691−3698.
(37) Eliseeva, S. V.; Bünzli, J.-C. G. *Chem. Soc. Rev.* **2010**, *39*, 189−227.
(38) (a) Borel, A.; Bean, J. F.; Clarkson, R. B.; Helm, L.; Moriggi, L.; Sherry, A. D.; Woods, M. *Chem.—Eur. J.* **2008**, *14*, 2658−2667. (b) Muller, G.; Kean, S. D.; Parker, D.; Riehl, J. P. *J. Phys. Chem. A* **2002**, *106*, 12349−12355.
(39) (a) Werts, M. H. V.; Jukes, R. T. F.; Verhoeven, J. W. *Phys. Chem. Chem. Phys.* **2002**, *4*, 1542−1548. (b) Kadjane, P.; Charbonnière, L. J.; Camerel, F.; Lainé, P.; Ziessel, R. *J. Fluoresc.* **2008**, *18*, 119−129.
(40) Nakamaru, K. *Bull. Chem. Soc. Jpn.* **1982**, *55*, 2697−2705.
(41) Beeby, A.; Clarkson, I. M.; Dickins, R. S.; Faulkner, S.; Parker, D.; Royle, L.; de Sousa, A. S.; Williams, J. A. G.; Woods, M. *J. Chem. Soc., Perkin Trans. 2* **1999**, 493−504.
(42) Supkowski, R. M.; Horrocks, W. D. W. Jr. *Inorg. Chim. Acta* **2002**, *340*, 44−48.
(43) Weibel, N.; Charbonnière, L. J.; Guardigli, M.; Roda, A.; Ziessel, R. *J. Am. Chem. Soc.* **2004**, *126*, 4888−4896.
(44) Peters, J. A.; Huskens, J.; Raber, D. J. *Prog. NMR Spectrosc.* **1996**, *28*, 283−350.
(45) Aime, S.; Barbero, L.; Botta, M.; Ermondi, G. *J. Chem. Soc., Dalton Trans.* **1992**, 225−228.
(46) Forsberg, J. H.; Delaney, R. M.; Zhao, Q.; Harakas, G.; Chandran, R. *Inorg. Chem.* **1995**, *34*, 3705−3715.
(47) Platas-Iglesias, C.; Roca-Sabio, A.; Regueiro-Figueroa, M.; Esteban-Gómez, D.; de Blas, A.; Rodríguez-Blas, T. *Curr. Inorg. Chem.* **2011**, *1*, 91−116.
(48) Dolg, M.; Stoll, H.; Savin, A.; Preuss, H. *Theor. Chim. Acta* **1989**, *75*, 173−194.
(49) (a) Corey, E. J.; Bailar, J. C. Jr. *J. Am. Chem. Soc.* **1959**, *81*, 2620−2629. (b) Beattie, J. K. *Acc. Chem. Res.* **1971**, *4*, 253−259.
(50) (a) Aime, S.; Botta, M.; Fasano, M.; Marques, M. P. M.; Geraldes, C. F. G. C.; Pubanz, D.; Merbach, A. E. *Inorg. Chem.* **1997**, *36*, 2059−2068. (b) Hoeft, S.; Roth, K. *Chem. Ber.* **1993**, *126*, 869−873. (c) Aime, S.; Botta, M.; Ermondi, G. *Inorg. Chem.* **1992**, *31*, 4291−4299.
(51) Parker, D.; Dickins, R. S.; Puschmann, H.; Crossland, C.; Howard, J. A. K. *Chem. Rev.* **2002**, *102*, 1977−2010.
(52) Purgel, M.; Baranyai, Z.; de Blas, A.; Rodríguez-Blas, T.; Bányai, I.; Platas-Iglesias, C.; Tóth, I. *Inorg. Chem.* **2010**, *49*, 4370−4382.
(53) (a) Regueiro-Figueroa, M.; Esteban-Gómez, D.; de Blas, A.; Rodríguez-Blas, T.; Platas-Iglesias, C. *Eur. J. Inorg. Chem.* **2010**, 3586−3595. (b) Di Vaira, M.; Stoppioni, P. *New J. Chem.* **2002**, *26*, 136−144. (c) Cosentino, U.; Villa, A.; Pitea, D.; Moro, G.; Barone, V.; Maiocchi, A. *J. Am. Chem. Soc.* **2002**, *124*, 4901−4909.
(54) Dunand, F. A.; Dickins, R. S.; Parker, D.; Merbach, A. E. *Chem.—Eur. J.* **2001**, *7*, 5160−5167.
(55) Gampp, H.; Maeder, M.; Meyer, C. J.; Zuberbühler, A. D. *Talanta* **1985**, *32*, 251−264.
(56) (a) Yee, E. L.; Gansow, O. A.; Weaver, M. J. *J. Am. Chem. Soc.* **1980**, *102*, 2278−2285. (b) Scarborough, R. M. Jr.; Smith, A. B. *J. Am. Chem. Soc.* **1977**, *99*, 7087−7089. (c) Luo, Y. R.; Byrne, R. H. *J. Solution Chem.* **2007**, *36*, 673−689.
(57) Dickins, R. S.; Parker, D.; Bruce, J. I.; Tozer, D. J. *Dalton Trans.* **2003**, 1264−1271.
(58) Aime, S.; Barge, A.; Benetollo, F.; Bombieri, G.; Botta, M.; Ugger, F. *Inorg. Chem.* **1997**, *36*, 4287−4289.
(59) (a) Lisowski, J.; Mazurek, J. *Polyhedron* **2002**, *21*, 811−816. (b) Brianese, N.; Casellato, U.; Tamburini, S.; Tomasen, P.; Vigato, P. A. *Inorg. Chem. Commun.* **1999**, *2*, 149−152.
(60) Wada, A.; Watanabe, M.; Yamanoi, Y.; Nishihara, H. *Chem. Commun.* **2008**, 1671−1673.
(61) Misteryukova, V. E.; Mikhailov, Yu. N.; Chuklanova, E. B.; Segeev, A. V.; Shchelokov, R. N. *Zh. Neorg. Khim.* **1998**, *43*, 1997−1998.
(62) (a) Evans, W. J.; Giarikos, D. G.; Johnston, M. A.; Greci, M. A.; Ziller, J. W. *J. Chem. Soc., Dalton Trans.* **2002**, 520−526. (b) Petrov, V. A.; Marshall, W. J.; Grushin, V. V. *Chem. Commun.* **2002**, 520−521.
(63) (a) Romanelli, M.; Kumar, G. A.; Emge, T. J.; Riman, R. E.; Brennan, J. G. *Angew. Chem., Int. Ed.* **2008**, *47*, 6049−6051. (b) Deacon, G. B.; Forsyth, C. M.; Junk, P. C.; Wang, J. *Chem.—Eur. J.* **2009**, *15*, 3082−3092. (c) Jayasundera, A. C. A.; Finch, A. A.; Townsend, P. D.; Lightfoot, P. *J. Mater. Chem.* **2007**, *17*, 4178−4183. (d) Deacon, G. B.; Meyer, G.; Stellfeldt, D. *Eur. J. Inorg. Chem.* **2000**, 1061−1071. (e) Zhou, W.; Xu, Y.; Han, L.; Zhu, D. *Dalton Trans.* **2010**, *39*, 3681−3686. (f) Deacon, G. B.; Fallon, G. D.; Forsyth, C. M.; Harris, S. C.; Junk, P. C.; Skelton, B. W.; White, A. H. *Dalton Trans.* **2006**, 802−812. (g) Deacon, G. B.; Evans, D. J.; Junk, P. C.; Lork, E.; Mews, R.; Zemva, B. *Dalton Trans.* **2005**, 2237−2238. (h) Xie, Z.; Chui, K.; Yang, Q.; Mak, T. C. W.; Sun, J. *Organometallics* **1998**, *17*, 3937−3944.
(64) (a) Parker, D.; Puschmann, H.; Batsanov, A. S.; Senanayake, K. *Inorg. Chem.* **2003**, *42*, 8646−8651. (b) Zhang, S.; Wu, K.; Biewer, M. C.; Sherry, A. D. *Inorg. Chem.* **2001**, *40*, 4284−4290. (c) Gunnlaugsson, T.; Davies, R. J. H.; Kruger, P. E.; Jensen, P.; McCabe, T.; Mulready, S.; O'Brien, J. E.; Stevenson, C. S.; Fanning, A.-M. *Tetrahedron Lett.* **2005**, *46*, 3761−3766.
(65) Chang, C. A.; Francesconi, L. C.; Malley, M. F.; Kumar, K.; Gougoutas, J. Z.; Tweedle, M. F. *Inorg. Chem.* **1993**, *32*, 3501.
(66) Thompson, A. L.; Parker, D.; Fulton, D. A.; Howard, J. A. K.; Pandya, S. U.; Puschmann, H.; Senanayake, K.; Stenson, P. A.; Badari, A.; Botta, M.; Avedano, S.; Aime, S. *Dalton Trans.* **2006**, 5605−5616.
(67) Zhang, S.; Michaudet, L.; Burgess, S.; Sherry, A. D. *Angew. Chem., Int. Ed.* **2002**, *41*, 1919−1921.
(68) Alderighi, L.; Bianchi, A.; Calabi, L.; Dapporto, P.; Giorgi, C.; Losi, P.; Paleari, L.; Paoli, P.; Rossi, P.; Valtancoli, B.; Virtuani, M. *Eur. J. Inorg. Chem.* **1998**, 1581−1584.
(69) Bianchi, A.; Calabi, L.; Giorgi, C.; Losi, P.; Mariani, P.; Paoli, P.; Rossi, P.; Valtancoli, B.; Virtuani, M. *J. Chem. Soc., Dalton Trans.* **2000**, 697−705.
(70) Amin, S.; Voss, D. A. Jr.; De Horrocks, W. Jr.; Lake, C. H.; Churchill, M. R.; Morrow, J. R. *Inorg. Chem.* **1995**, *34*, 3294−3300.
(71) Bombieri, G.; Marchini, N.; Ciattini, S.; Mortillaro, A.; Aime, S. *Inorg. Chim. Acta* **2006**, *359*, 3405−3411.
(72) Millar, K. J.; Saherwala, A. A.; Webber, B. C.; Wu, Y.; Sherry, A. D.; Woods, M. *Inorg. Chem.* **2010**, *49*, 8662−8664.
(73) Glasoe, P. K.; Long, F. A. *J. Phys. Chem.* **1960**, *64*, 188−190.
(74) (a) *CrysAlis CCD*, version 1.171.33.52; Oxford Diffraction Ltd.: Oxford, U.K., 2009; release 06-11-2009 CrysAlis171.NET. (b) *CrysAlis RED*, version 1.171.33.52; Oxford Diffraction Ltd.: Oxford, U.K., 2009; release 06-11-2009 CrysAlis171.NET.

(75) *SHELX*: Sheldrick, G. M. *Acta Crystallogr.* **2008**, *A64*, 112−122.
(76) *WinGX* MS-Windows system of programs for solving, refining and analysing single crystal X-ray diffraction data for small molecules: Farrugia, L. J. *J. Appl. Crystallogr.* **1999**, *32*, 837−838.
(77) Sheldrick, G. M. *SADABS*, version 2.10; University of Göttingen: Göttingen, Germany, 2004.
(78) Herbst-Irmer, R.; Sheldrick., G. M. *Acta Crystallogr.* **1998**, *B54*, 443−449.
(79) *SIR97*: Altomare, A.; Burla, M. C.; Camalli, M.; Cascarano, G. L.; Giacovazzo, C.; Guagliardi, A.; Moliterni, A. G. G.; Polidori, G.; Spagna, R. *J. Appl. Crystallogr.* **1999**, *32*, 115−119.
(80) Becke, A. D. *J. Chem. Phys.* **1993**, *98*, 5648−5652.
(81) Lee, C.; Yang, W.; Parr, R. G. *Phys. Rev. B* **1988**, *37*, 785−789.
(82) Frisch, M. J.; Trucks, G. W.; Schlegel, H. B.; Scuseria, G. E.; Robb, M. A.; Cheeseman, J. R.; Scalmani, G.; Barone, V.; Mennucci, B.; Petersson, G. A.; Nakatsuji, H.; Caricato, M.; Li, X.; Hratchian, H. P.; Izmaylov, A. F.; Bloino, J.; Zheng, G.; Sonnenberg, J. L.; Hada, M.; Ehara, M.; Toyota, K.; Fukuda, R.; Hasegawa, J.; Ishida, M.; Nakajima, T.; Honda, Y.; Kitao, O.; Nakai, H.; Vreven, T.; Montgomery, J. A., Jr.; Peralta, J. E.; Ogliaro, F.; Bearpark, M.; Heyd, J. J.; Brothers, E.; Kudin, K. N.; Staroverov, V. N.; Kobayashi, R.; Normand, J.; Raghavachari, K.; Rendell, A.; Burant, J. C.; Iyengar, S. S.; Tomasi, J.; Cossi, M.; Rega, N.; Millam, N. J.; Klene, M.; Knox, J. E.; Cross, J. B.; Bakken, V.; Adamo, C.; Jaramillo, J.; Gomperts, R.; Stratmann, R. E.; Yazyev, O.; Austin, A. J.; Cammi, R.; Pomelli, C.; Ochterski, J. W.; Martin, R. L.; Morokuma, K.; Zakrzewski, V. G.; Voth, G. A.; Salvador, P.; Dannenberg, J. J.; Dapprich, S.; Daniels, A. D.; Farkas, Ö.; Foresman, J. B.; Ortiz, J. V.; Cioslowski, J.; Fox, D. J. *Gaussian 09*, revision A.01; Gaussian, Inc.: Wallingford, CT, 2009.
(83) (a) Maron, L.; Eisenstein, O. *J. Phys. Chem. A* **2000**, *104*, 7140−7143. (b) Boehme, C.; Coupez, B.; Wipff, G. *J. Phys. Chem. A* **2002**, *106*, 6487−6498.
(84) Vetere, V.; Maldivi, P.; Adamo, C. *J. Comput. Chem.* **2003**, *24*, 850−858.
(85) (a) Peng, C.; Ayala, P. Y.; Schlegel, H. B.; Frisch, M. J. *J. Comput. Chem.* **1996**, *17*, 49−56. (b) Peng, C.; Schlegel, H. B. *Isr. J. Chem.* **1994**, *33*, 449−454.